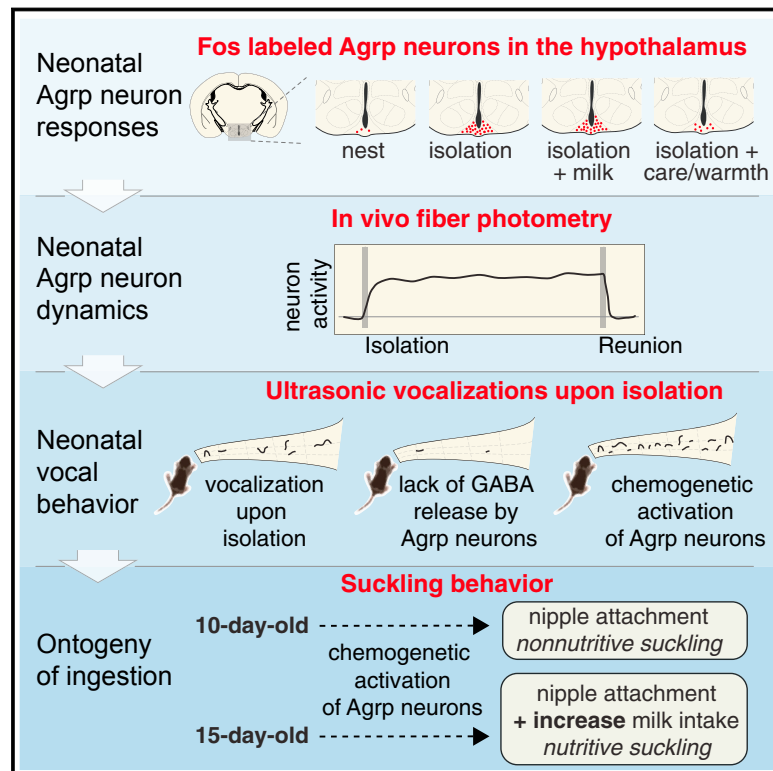


Functional Ontogeny of Hypothalamic Agrp Neurons in Neonatal Mouse Behaviors

Graphical Abstract



Authors

Marcelo R. Zimmer,
Antonio H.O. Fonseca, Onur Iyilikci,
Rafael Dai Pra, Marcelo O. Dietrich

Correspondence

marcelo.dietrich@yale.edu

In Brief

Hypothalamic Agrp neurons play a role in offspring-to-caregiver bonding independent of their role in food ingestion.

Highlights

- Isolation from the nest activates Agrp neurons in neonatal mice
- Care and warmth, but not milk, blunts activation of Agrp neurons
- Neonatal Agrp neurons modulate isolation-induced ultrasonic vocalizations
- Agrp neurons increase milk ingestion in 15- but not in 10-day-old mice



Functional Ontogeny of Hypothalamic Agrp Neurons in Neonatal Mouse Behaviors

Marcelo R. Zimmer,^{1,3} Antonio H.O. Fonseca,^{1,4} Onur Iyilikci,¹ Rafael Dai Pra,^{1,3} and Marcelo O. Dietrich^{1,2,3,5,*}

¹Program in Integrative Cell Signaling and Neurobiology of Metabolism, Department of Comparative Medicine, Yale University School of Medicine, New Haven, CT 06520, USA

²Department of Neuroscience, Yale University School of Medicine, New Haven, CT 06520, USA

³Graduate Program in Biological Sciences-Biochemistry, Universidade Federal do Rio Grande do Sul, Porto Alegre, RS 90035, Brazil

⁴Graduate Program in Microelectronics, Universidade Federal do Rio Grande do Sul, Porto Alegre, RS 15064, Brazil

⁵Lead Contact

*Correspondence: marcelo.dietrich@yale.edu

<https://doi.org/10.1016/j.cell.2019.04.026>

SUMMARY

Hypothalamic Agrp neurons regulate food ingestion in adult mice. Whether these neurons are functional before animals start to ingest food is unknown. Here, we studied the functional ontogeny of Agrp neurons during breastfeeding using postnatal day 10 mice. In contrast to adult mice, we show that isolation from the nursing nest, not milk deprivation or ingestion, activated Agrp neurons. Non-nutritive suckling and warm temperatures blunted this effect. Using *in vivo* fiber photometry, neonatal Agrp neurons showed a rapid increase in activity upon isolation from the nest, an effect rapidly diminished following reunion with littermates. Neonates unable to release GABA from Agrp neurons expressed blunted emission of isolation-induced ultrasonic vocalizations. Chemogenetic overactivation of these neurons further increased emission of these ultrasonic vocalizations, but not milk ingestion. We uncovered important functional properties of hypothalamic Agrp neurons during mouse development, suggesting these neurons facilitate offspring-to-caregiver bonding.

INTRODUCTION

Agouti-related peptide (Agrp) neurons in the arcuate nucleus of the hypothalamus serve as a central coordinator to regulate food intake. Ablation of these neurons leads to aphagia in adult mice (Gropp et al., 2005; Luquet et al., 2005), but not in neonates, suggesting that Agrp neurons do not contribute to ingestive behaviors early in development. In support of this view, Agrp neurons show delayed development in rodents (Nilsson et al., 2005; Padilla et al., 2010), when the final maturation of Agrp neuronal circuitry coincides with weaning (Grove and Smith, 2003). However, impairing development of Agrp neurons during the first postnatal week in mice has persistent consequences to metabolism and behavior (Dietrich et al., 2012; Joly-Amado

et al., 2012), suggesting an unidentified function for Agrp neurons during early development.

Here, we assessed the functional ontogeny of Agrp neurons in early postnatal development of mice at postnatal day 10 (P10) and during the weaning period during postnatal days 15–21 (P15–P21).

RESULTS

Isolation from the Nursing Nest, Not Nutrient Intake, Activates Agrp Neurons in Neonates

In adult mice, nutrient deprivation activates Agrp neurons (Hahn et al., 1998; Takahashi and Cone, 2005). So, we investigated the extent to which Agrp neurons respond to a lack of nutrients in neonatal mice. To test this, we isolated P10 mice from the nest for 90 min or 8 h to prevent nutrient intake via milk ingestion (Figure 1A). A 90-min time from onset of separation maximizes Fos expression (Barros et al., 2015). Both periods of isolation increased Agrp neuronal activity, as indicated by the increased number of Fos positive Agrp neurons upon isolation (nest: $3.14 \pm 0.96\%$, $n = 9$; isolation/90 min: $31.19 \pm 1.89\%$, $n = 10$; isolation/8 h: $46.19 \pm 2.04\%$, $n = 3$; $F_{2, 19} = 128.6$, $p < 10^{-11}$, one-way ANOVA; Figures 1B–1D).

Because 90 min significantly increased Fos positive Agrp neurons, we tested whether this period of isolation also stimulated milk intake. We measured milk intake by calculating the change in body weight in animals that remained in the nest for 90 min compared to animals isolated for 90 min followed by re-introduction to the nest for an additional 90-min period (Figure 1E). In this protocol, we did not observe significant differences in the body-weight changes between the two experimental conditions (nest: 62.1 ± 15.4 mg, $n = 12$; reunion: 76.2 ± 14.4 mg, $n = 12$; $t_{22} = 0.65$, $p = 0.51$, unpaired t test; Figure 1F). Thus, activation of Agrp neurons after 90 min of isolation from the nest in P10 mice is not significant to increase milk intake. Moreover, the increased activation of Agrp neurons does not seem to arise from a generalized stress response, as corticosterone levels did not increase after isolation (nest: 9.96 ± 1.85 ng/mL, $n = 7$; isolation: 12.40 ± 1.85 ng/mL, $n = 11$; $t_{16} = 0.88$, $p = 0.39$, unpaired t test; Figure 1G), and testing pups in the presence of a predator odor for 90 min did not alter Fos labeling in Agrp neurons (nest: $1.19 \pm 0.92\%$, $n = 2$; isolation: $23.82 \pm 4.78\%$,



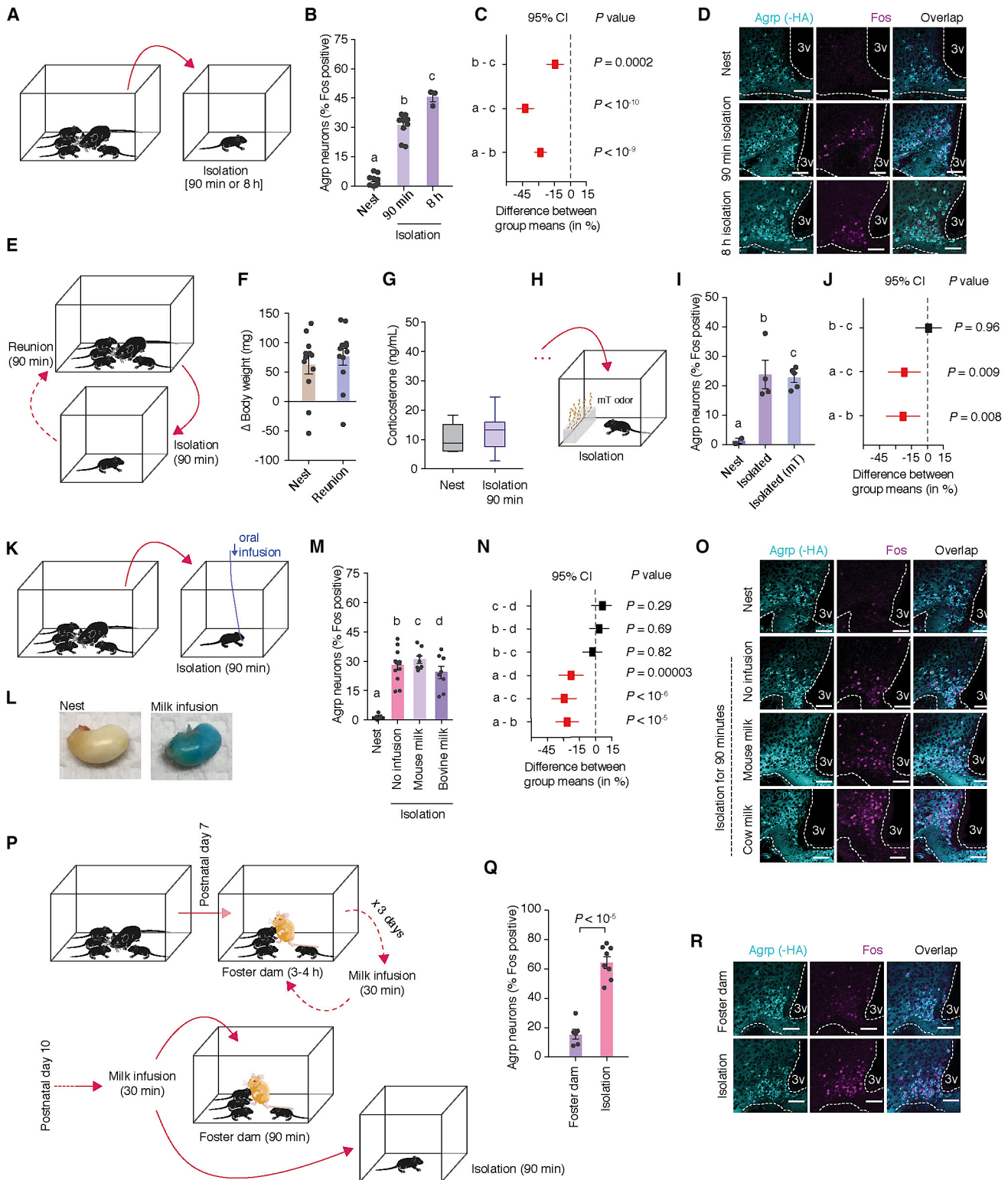


Figure 1. Fos Labels Agpr Neuron Activation in P10 Mice upon Social Isolation

(A) P10 mice were socially isolated for 90 min or 8 h.

(B) Agpr neurons positive for Fos immunoreactivity (nest, $n = 9$; isolation/90 min, $n = 10$; isolation/8 h, $n = 3$, one-way ANOVA, $p < 10^{-11}$).

(legend continued on next page)

$n = 4$; isolation and predator odor: $22.71 \pm 1.59\%$, $n = 5$; $F_{2, 8} = 9.73$, $p = 0.007$, one-way ANOVA; Figures 1H–1J).

To evaluate whether the activation of *Agrp* neurons upon isolation from nest is due to caloric deprivation, we isolated P10 mice while orally infusing bovine or mouse derived milk (Figure 1K). We confirmed milk ingestion by adding a colored dye to the milk to verify its presence in the stomach (Figure 1L). Surprisingly, our results showed no significant difference between the activation of *Agrp* neurons between the groups that received an oral infusion of milk and the control group that received a passive oral probe with no milk infusion (nest: $1.51 \pm 0.65\%$, $n = 5$; isolation and no infusion: $27.88 \pm 2.39\%$, $n = 12$; isolation and mouse milk: $30.73 \pm 1.93\%$, $n = 8$; isolation and bovine milk: $24.24 \pm 3.14\%$, $n = 8$; $F_{3, 29} = 19.38$, $p < 10^{-6}$, one-way ANOVA; Figures 1M–1O).

Next, we tested the hypothesis that *Agrp* neuron activity in P10 mice increases upon separation in anticipation of future nutrient deprivation. To this end, we investigated the extent to which isolation from the nest activates *Agrp* neurons when dissociating milk intake and the nest. P7 mice were housed with a foster non-lactating dam and were manually fed milk by an investigator (Figure 1P). All neonates quickly developed locomotor activity toward the investigator at feeding onset, which suggests a learned association that the milk source was outside the home nest. We then assessed activation of *Agrp* neurons at P10 at either isolation or return to the home cage with the foster dam for a period of 90 min after all pups were previously fed with equal volumes of milk. Similar to our previous experiments, isolation from the home nest strongly increased the number of Fos positive *Agrp* neurons compared to mice that returned to the home cage (foster dam: $15.59 \pm 3.26\%$, $n = 6$; isolation: $64.39 \pm 3.94\%$, $n = 8$; $t_{12} = 9.06$, $p < 10^{-5}$, unpaired t test; Figures 1Q and 1R). Taken together, these results suggest that activation of *Agrp* neurons in P10 mice following isolation from the nest does not require milk

deprivation or anticipation of milk deprivation, which stands in contrast to adult mice.

Non-nutritive Suckling and Thermal Support Blunt *Agrp* Neuron Activation in Neonates

Our next goal was to evaluate the relative importance of different components of the nest environment and mother-infant interaction that contribute to *Agrp* neuron activation in P10 mice after isolation from the nest. In the nursing nest, pups receive care from the dam. An important feature of maternal care is neonatal attachment to the mother's nipple and suckling. So, we investigated the extent to which suckling alters the activation of *Agrp* neurons. We fostered P10 mice with non-lactating dams, non-lactating dams with protruded nipples, and lactating dams (Figure 2A). In all cases, foster dams promptly retrieved the pups and placed them in the nest. All foster dams displayed maternal behaviors, such as grooming and licking and arched-back "nursing" of pups, as expected. Interestingly, all foster dams blunted the activation of *Agrp* neurons in P10 mice compared to isolated pups (nest: $2.10 \pm 0.21\%$, $n = 6$; isolation: $26.47 \pm 1.57\%$, $n = 6$; non-lactating foster dam: $16.59 \pm 1.64\%$, $n = 7$; non-lactating foster dam with protruded nipples: $8.66 \pm 1.26\%$, $n = 6$; lactating foster dam: $10.29 \pm 0.65\%$, $n = 4$; $F_{4, 24} = 50.29$, $p < 10^{-10}$, one-way ANOVA; Figures 2B and 2C). Attachment of pups to the foster dam's nipples further decreased the number of Fos-labeled *Agrp* neurons compared to pups placed with a foster dam with non-protruded nipples to prevent nipple attachment (Figures 2B and 2C). The effect of nipple attachment was irrespective of milk availability, as the expression of Fos in pups showed a similar magnitude when placed with lactating and non-lactating foster dams with protruded nipples (Figures 2B and 2C). Overall, activation of *Agrp* neurons in P10 mice is blunted by non-nutritive suckling, an important component of maternal care, and is not further reduced by availability of milk in the dam's nipples.

(C) Tukey-Kramer's multiple comparisons test of the difference between means (95% confidence intervals from B), representing effect sizes.

(D) Representative images of immunohistochemistry for HA (cyan, labels *Agrp*^{Rp122-HA} mice), Fos (magenta), and overlap. Scale bars represent 50 μ m.

(E) Effect of isolation (90 min) on milk intake upon reunion with the dam and litter for an additional 90 min.

(F) Delta body weight as a measure of milk intake during 90 min in P10 mice (control, $n = 12$; reunion, $n = 12$, unpaired t test, $p = 0.51$).

(G) Plasma corticosterone levels in P10 mice after 90-min isolation (control, $n = 7$; reunion, $n = 11$, unpaired t test, $p = 0.39$). Boxplot represents median, 1st/3rd quartiles, and min and max values.

(H) Effect of exposure to predator odor (mT) during 90-min isolation in P10 mice.

(I) Quantification of *Agrp* neurons positive for Fos (nest, $n = 2$; isolation, $n = 4$; isolation/mT, $n = 5$, one-way ANOVA, $p = 0.007$).

(J) Tukey-Kramer's multiple comparisons test of the difference between means (95% confidence intervals from I), representing effect sizes.

(K) Effect of milk infusion (mouse or bovine) in the activation of *Agrp* neurons in isolated P10 mice.

(L) Infused milk was labeled with a blue dye to confirm ingestion. Post-mortem images of the stomach of P10 mice.

(M) Quantification of *Agrp* neurons positive for Fos (nest, $n = 5$; isolation with no infusion, $n = 12$; isolation with infusion of mouse milk, $n = 8$; isolation with infusion of cow milk, $n = 8$, one-way ANOVA, $p < 10^{-6}$).

(N) Tukey-Kramer's multiple comparisons test of the difference between means (95% confidence intervals from M), representing effect sizes.

(O) Representative images of immunohistochemistry for HA (cyan, labeling *Agrp*^{Rp122-HA} mice), Fos (magenta), and overlap. Scale bars represent 50 μ m.

(P) Effect of artificial rearing mice on Fos upon isolation. P7 mice were fostered with a non-lactating dam, while hand-fed every 3–4 h for 3 days. At P10, all mice were hand-fed and separated in two groups: reunited with the foster dam or isolated for 90 min.

(Q) Quantification of *Agrp* neurons positive for Fos (foster dam, $n = 6$; isolation, $n = 8$, unpaired t test, $p < 10^{-5}$).

(R) Representative images of immunohistochemistry for HA (cyan, labeling *Agrp*^{Rp122-HA} mice), Fos (magenta), and overlap. Scale bars represent 50 μ m.

In (B), (F), (I), (M), and (Q), bars indicate mean \pm SEM. Circles represent individual values. In (C), (J) and (N), symbols represent mean \pm SEM; red denotes statistically significant differences.

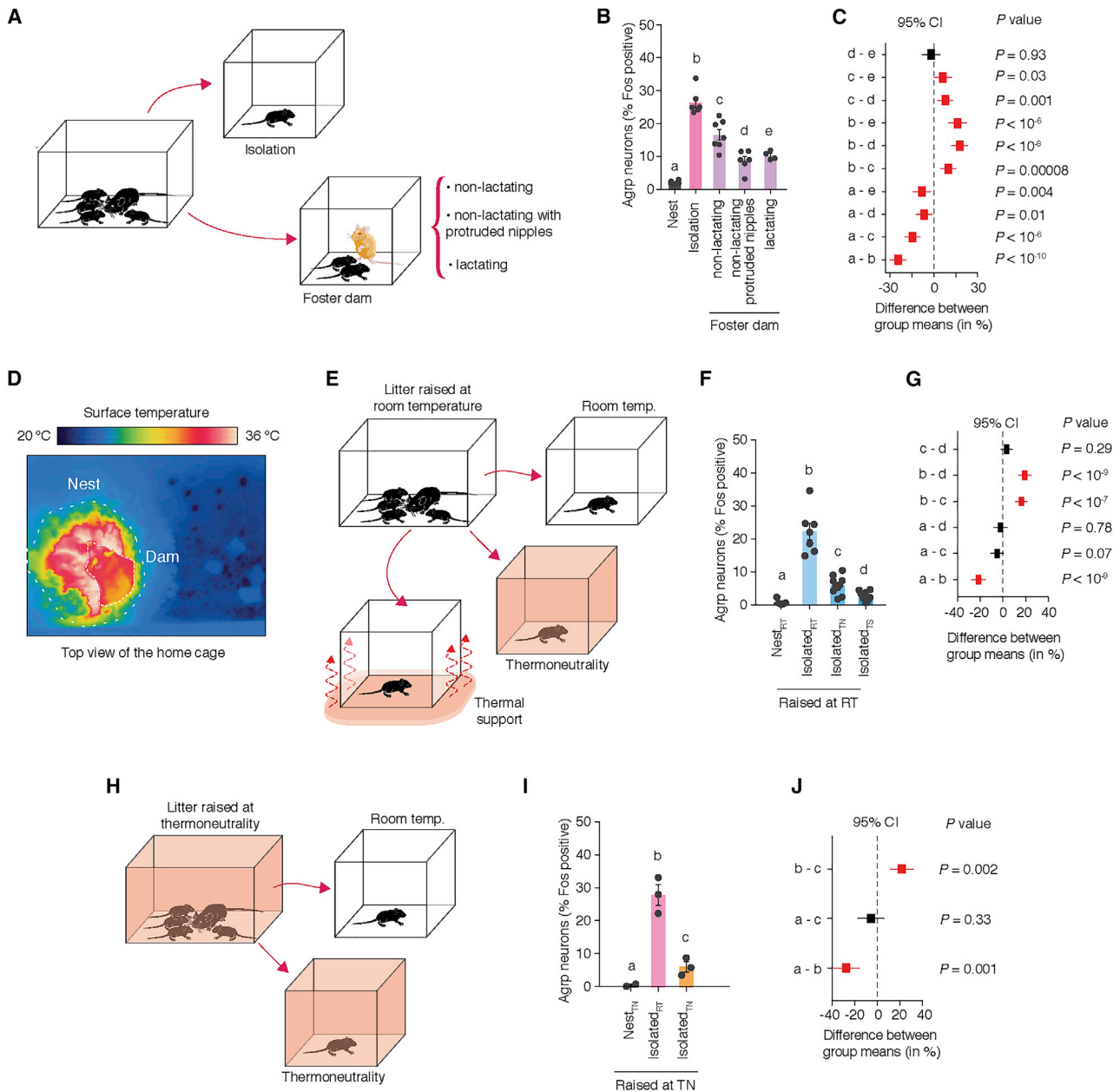


Figure 2. Warm Temperatures Blunt Activation of AgRP Neurons in P10 Mice

(A) Study design: P10 mice were either fostered with non-lactating dams, with non-lactating dams with protruded nipples, or with lactating dams for 90 min. A control group was not manipulated (nest) and a second group was isolated (isolation).

(B) Quantification of AgRP neurons positive for Fos (nest, $n = 6$; isolation, $n = 6$; non-lactating foster dam, $n = 7$; non-lactating foster dam with protruded nipples, $n = 6$; lactating foster dam, $n = 4$, one-way ANOVA, $p < 10^{-10}$).

(C) Tukey-Kramer's multiple comparisons test of the difference between means (95% confidence intervals from B), representing effect sizes.

(D) Thermo-photography of the nursing nest. Lactating dam is on the top of P10 offspring. Nest temperature is approximately 34°C – 36°C .

(E) Offspring raised at room temperature (RT) were isolated either at room temperature, at thermoneutrality (TN, in a climate chamber set to 35°C) or at room temperature with a thermal support (TS) irradiating heat from underneath the cage ($\approx 35^{\circ}\text{C}$).

(F) Quantification of AgRP neurons positive for Fos (nest and room temperature, $n = 5$; isolation and room temperature, $n = 10$; isolation and thermal support, $n = 8$, one-way ANOVA, $p = 10^{-10}$).

(G) Tukey-Kramer's multiple comparisons test of the difference between means (95% confidence intervals from F) representing effect sizes.

(H) Offspring raised at thermoneutrality (climate chamber at 35°C) were isolated for 90 min at room temperature or thermoneutrality.

(legend continued on next page)

The nursing nest provides critical thermal insulation, which reduces heat loss from neonates that have not fully developed homeostatic mechanisms for thermoregulation. Dams contribute to thermal insulation by building a nest and skin-to-skin contact with pups (Figure 2D). To test the effects of thermal insulation on the activation of *Agrp* neurons, we isolated P10 mice at room temperature or at a thermoneutral temperature ($\approx 35^\circ\text{C}$; Figure 2E). Because temperature exchanges in the nest occur by skin-to-skin contact, we included an additional control group, in which we provided thermal support by irradiating heat ($\approx 35^\circ\text{C}$) from underneath (Figure 2E). 90 min of isolation at thermoneutrality or with thermal support strongly suppressed activation of *Agrp* neurons in P10 mice as assayed by Fos labeling compared with pups isolated at room temperature (nest: $0.77 \pm 0.39\%$, $n = 5$; isolation and room temperature: $22.19 \pm 2.53\%$, $n = 7$; isolation and thermoneutrality: $5.90 \pm 0.86\%$, $n = 10$; isolation and thermal support: $2.75 \pm 0.51\%$, $n = 8$; $F_{3,26} = 47.31$, $p = 10^{-10}$, one-way ANOVA; Figures 2F and 2G). Thus, *Agrp* neurons in P10 mice respond to the withdrawal of thermal insulation when isolated from the nursing nest. This factor holds primary importance for the responses of these neurons to isolation.

Next, we tested the extent to which the response of *Agrp* neurons in P10 mice to the withdrawal of thermal insulation was dependent on prior experience with drops in ambient temperature. To prevent mice from experiencing ambient temperatures lower than nest temperatures, we repeated the experiments in animals born and raised in a thermoneutral environment (Figure 2H). P10 mice raised at thermoneutrality showed increased Fos-labeled *Agrp* neurons when isolated at room temperature but not at thermoneutrality (nest and thermoneutrality: $0.62 \pm 0.33\%$, $n = 2$; isolation and room temperature: $27.94 \pm 3.13\%$, $n = 3$; isolation and thermoneutrality: $6.16 \pm 1.54\%$, $n = 3$; $F_{2,5} = 37.91$, $p = 0.001$, one-way ANOVA; Figures 2I and 2J). Thus, the response of *Agrp* neurons to withdrawal of thermal insulation in P10 mice does not require previous experiences with drops in ambient temperature.

Neonatal *Agrp* Neurons Undergo Rapid Activity Changes

In the previous experiments, we could not elucidate the temporal dynamics of physiological activation of *Agrp* neurons. For example, *Agrp* neurons after isolation (Figure 3A) could slowly increase their activity similar to a homeostat (Figure 3B). Alternatively, these neurons could rapidly respond to isolation (Figure 3C) similar to an alarm and reflexive system. A third alternative suggests that *Agrp* neurons could show delayed activation (Figure 3D), suggesting a thresholding mechanism triggers these neurons in neonates.

To better understand the natural activity dynamics of *Agrp* neurons early in postnatal development, we injected an adeno-associated virus encoding jRCaMP7s in a Cre-dependent manner in newborn *Agrp*^{Cre/Cre} mice (Figures 3E–G) (Dana

et al., 2018). We then used fiber photometry to measure calcium transients originating from *Agrp* neurons upon isolation-reunion in P13–14 pups (Figure 3A). We found that pup isolation from the nest increased activity of *Agrp* neurons that occurred within seconds (Figures 3H and 3I) and persisted throughout the isolation period (10 min). After this initial separation, reunion of the isolated animal with the litter immediately decreased the activity of *Agrp* neurons (Figures 3H and 3I). The suppression of *Agrp* neuronal activity was robust and rapid, normalizing the detected signal to pre-isolation levels in less than 30 s (Figures 3H and 3I). All animals tested showed this response to isolation-reunion, suggesting a general model in which *Agrp* neurons in neonates rapidly respond to disruptions in the nest conditions (Figure 3C).

Neonatal *Agrp* Neurons Modulate the Emission of Ultrasonic Vocalizations

In most neonatal mammals, including mice, disruptions in the nest condition lead to infant vocalization (Hofer, 1994). In mice and rats, neonates emit ultrasonic vocalizations (USVs) when separated from the dam (Noirot, 1966, 1968; Zippelius and Schleidt, 1956) (Figures 4A and 4B). We investigated whether activation of *Agrp* neurons in neonates upon isolation from the nest could modulate emission of USVs.

First, we confirmed that isolation from the nest induced vocal behavior in P10 mice (Figure 4A). We then investigated whether isolation at thermoneutrality would influence USVs, since these conditions blunt activation of *Agrp* neurons upon isolation (Figure 2). Analysis of vocal behavior showed a rapid increase in USV emission upon isolation from the nest (Figures 4B–4E), an effect that blunted at thermoneutrality (nest, $n = 3$; isolated and room temperature, $n = 16$; isolated and thermoneutrality, $n = 4$; $F_{2,20} = 18.08$, $p < 10^{-4}$, one-way ANOVA; Figures 4C–4E). Thus, vocal behavior dynamics in neonatal mice follow the dynamics of *Agrp* neuron activation upon isolation in these experimental conditions.

To test the extent to which *Agrp* neurons contribute to vocal behavior of P10 mice upon isolation, we tested animals lacking the transmitters released by *Agrp* neurons (NPY and GABA) (Hahn et al., 1998; Horvath et al., 1997). We recorded the emission of USVs in *Npy*^{KO} and *Agrp*^{Vgat-KO} mice and their littermate controls following 10 minutes isolation in P10 mice. Animals lacking NPY exhibited a similar number of USVs after isolation compared to controls (control: 343.4 ± 56.8 USVs, $n = 12$; *Npy*^{KO/+}: 384.5 ± 69.3 USVs, $n = 17$; *Npy*^{KO/KO}: 348.0 ± 91.7 USVs, $n = 7$; $p = 0.74$, Kruskal-Wallis [KW] test; Figure 4F). In contrast, *Agrp*^{Vgat-KO} mice had a significant decrease in emission of USVs upon isolation (control: 321.0 ± 50.4 USVs, $n = 10$; *Agrp*^{Vgat-KO}: 57.7 ± 14.6 USVs, $n = 14$; $U = 2$, $p < 10^{-5}$, Mann-Whitney test; Figures 4G and 4H).

We further analyzed the spectro-temporal characteristics of 3,427 USVs from control mice and 786 USVs from *Agrp*^{Vgat-KO} mice. We characterized individual USVs by changes in

(I) Quantification of *Agrp* neurons positive for Fos (nest and thermoneutrality, $n = 2$; isolation and room temperature, $n = 3$; isolation and thermoneutrality, $n = 3$, one-way ANOVA, $p = 0.001$).

(J) Tukey-Kramer's multiple comparisons test of the difference between means (95% confidence intervals from I), representing effect sizes.

In (B), (F), and (I), bars represent mean \pm SEM; round symbols represent individual values. In (C), (G), and (J), symbols represent mean \pm SEM; red denotes statistically significant differences.

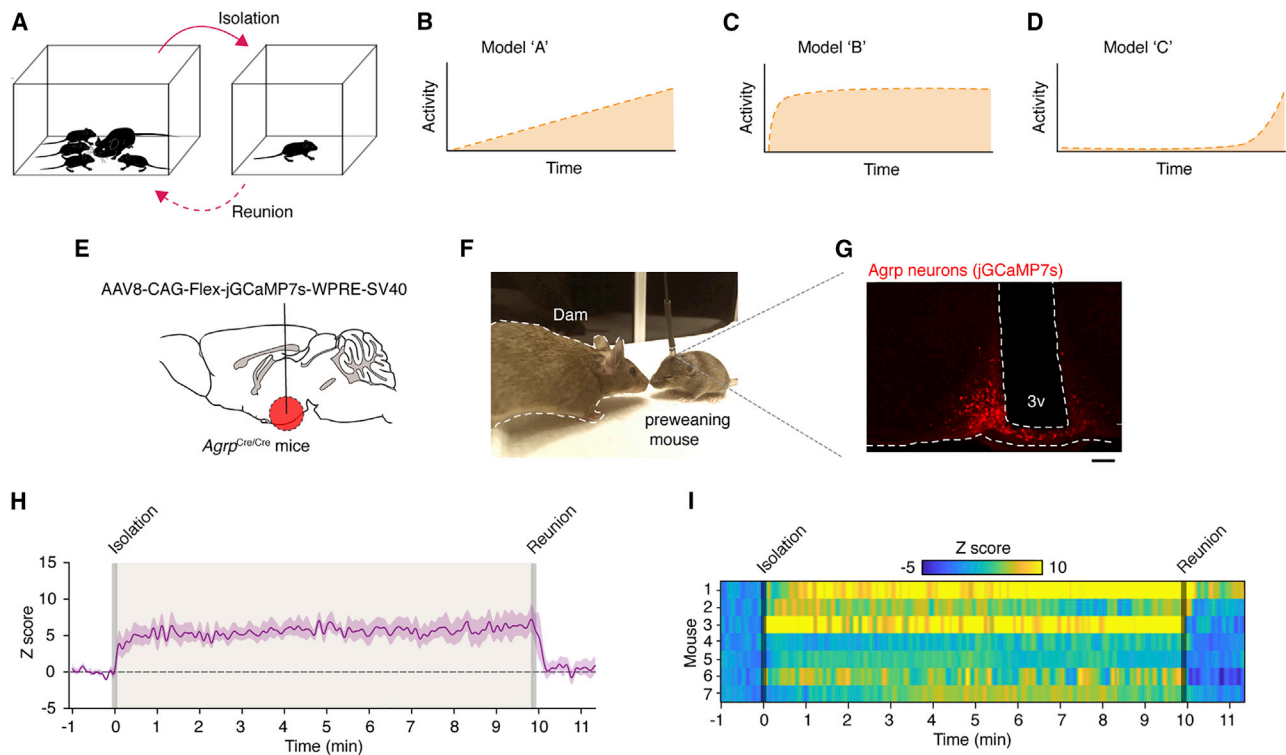


Figure 3. Rapid Dynamics of Agrp Neuronal Activity in Mice during Early Development

(A) Experimental model of isolation and reunion in neonates, which activates Agrp neurons after 90 min. Three theoretical models of activity changes of these neurons are illustrated in (B)–(D).

(B) Model A: activity of Agrp neurons gradually increases during the 90-min isolation.

(C) Model B: activity of Agrp neurons rapidly increases upon isolation.

(D) Model C: activity of Agrp neurons increases in isolation after a delay.

(E) In newborn *Agrp^{Cre/Cre}* mice, an adeno-associated virus was injected in the arcuate nucleus of the hypothalamus to express jGCaMP7s in Agrp neurons (AAV-CAG-Flex-jGCaMP7s).

(F) Preweaning mouse connected to an optic fiber and its dam.

(G) Expression of jGCaMP7s in Agrp neurons of a P14 mouse.

(H) Z score of Agrp neuronal activity in P13–14 mice. Baseline was recorded for 1 min and then pups were isolated for 10 min. Subsequently, pups were reunited with the litter. Plot represents mean \pm SEM ($n = 7$ animals).

(I) Heat plot representing individual responses to isolation and reunion.

spectro-temporal characteristics, such as duration, frequency, and bandwidth. Compared to control mice, USVs from *Agrp^{Vgat-KO}* mice decreased in duration of 9.5 ms (control: 37.84 ± 0.45 ms; *Agrp^{Vgat-KO}*: 28.31 ± 0.84 ms; $D = 0.176$, $p = 10^{-15}$, Kolmogorov-Smirnov [KS] test; Figure 4I), in mean frequency of 1.9 kHz (control: 82.20 ± 0.28 kHz; *Agrp^{Vgat-KO}*: 80.24 ± 0.55 kHz; $D = 0.10$, $p = 10^{-15}$, KS test; Figure 4J), and in bandwidth of 5.6 kHz (control: 22.86 ± 0.35 kHz; *Agrp^{Vgat-KO}*: 17.20 ± 0.67 kHz; $D = 0.17$, $p = 10^{-15}$, KS test; Figure 4K). We also found an overall decrease in the number of vocalizations across most USV categories (Figures 4L–4X) (Grimsley et al., 2011). However, we observed an increase in the incidence of “short” vocalizations, when analyzing the relative frequency of USV categories (Figure 4Y). This syllable represents the simplest form of vocalization by neonatal mice based on spectro-temporal characteristics (Figures 4L–4V). Thus, lacking GABA release from Agrp neurons, P10 *Agrp^{Vgat-KO}* mice led to fewer and simpler USVs compared to control animals.

Taken together, these findings indicate Agrp neurons are critically positioned to modulate the emission of USVs in neonatal mice.

Chemogenetic Activation of Agrp Neurons Increases USV Emission

We further tested whether chemogenetic activation of Agrp neurons could modulate emission of USV in isolated P10 pups using *Agrp^{Trpv1}* mice (Dietrich et al., 2015; Ruan et al., 2014; Arenkiel et al., 2008; Güler et al., 2012) (Figure 5A; Figure S1). Subcutaneous injection of capsaicin (10 mg/kg) in *Agrp^{Trpv1}* mice robustly activated Agrp neurons in young pups (Figure 5B; $n = 5$ mice per group; $U = 0$, $p = 0.004$, Mann-Whitney test). Chemogenetic activation of Agrp neurons using the *Agrp^{Trpv1}* animal model induced a 61% increase in USV emission in P10 mice (control: 686.7 ± 50.22 USVs, $n = 32$; *Agrp^{Trpv1}*: 1040.0 ± 66.56 USVs, $n = 24$; $t_{51} = 4.318$, $p < 0.0001$; 2-tailed unpaired t test; Figures 5C–5E).

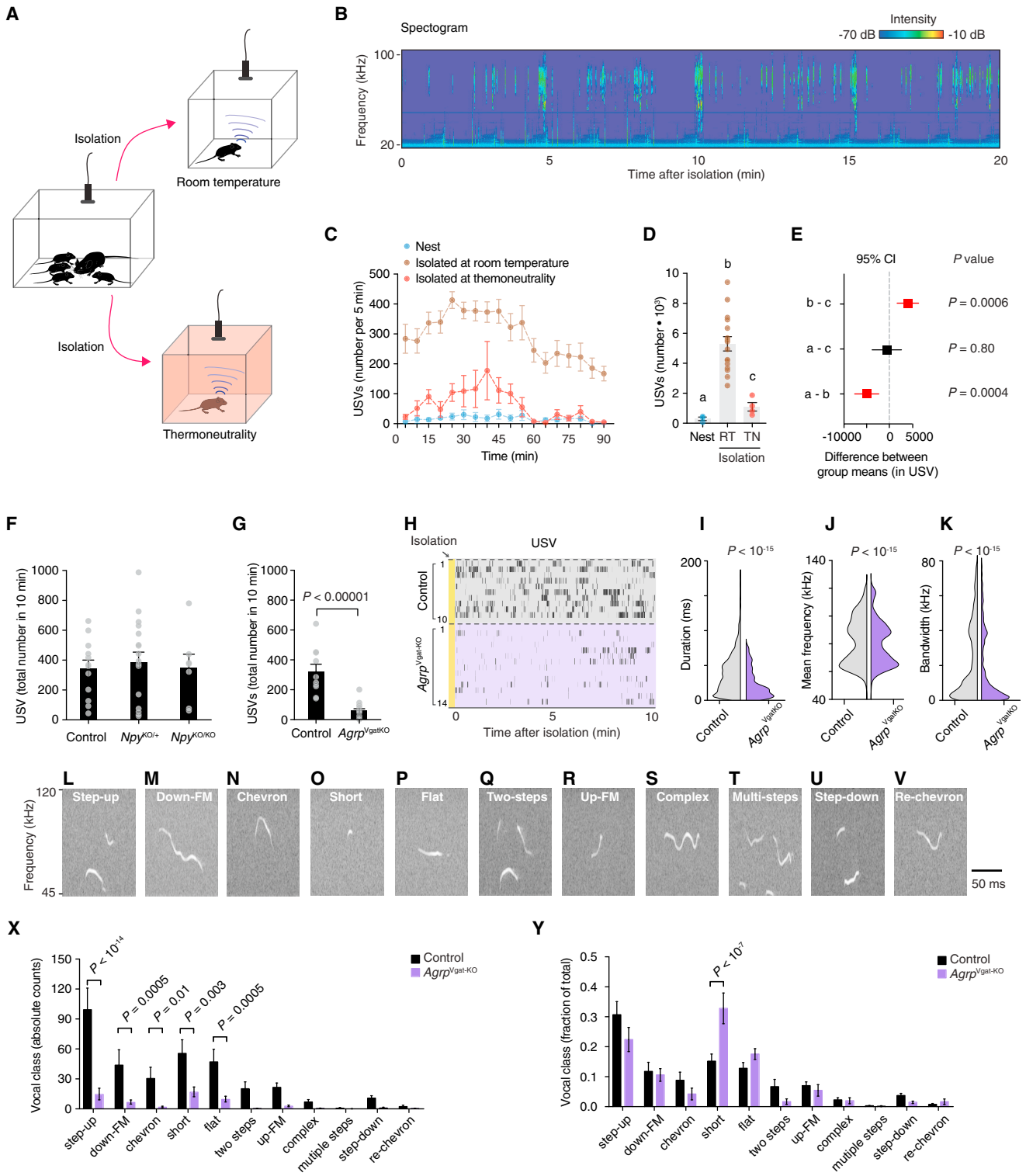


Figure 4. Agrp Neurons in P10 Mice Modulate Emission of Ultrasonic Vocalizations via GABA Release

(A) Experimental model of isolation in P10 mice at room temperature (RT) or at thermoneutral conditions (thermoneutrality; climate chamber set at 35°C). (B) Representative spectrogram of ultrasonic vocalizations (USVs) in P10 mice recorded in isolation. (C) Number of USVs in five-minute bins during isolation at room temperature or thermoneutrality and control group recorded in the nest.

(legend continued on next page)

We also analyzed the spectro-temporal characteristics of a total of 21,019 USVs from control mice and 24,976 vocalizations from *Agrp^{Trpv1}* mice. Upon activation of *Agrp* neurons, the USV duration decreased by 4 ms (control: 51.42 ± 0.23 ms; *Agrp^{Trpv1}*: 47.09 ± 0.19 ms; $D = 0.077$, $p = 10^{-15}$, KS test; Figure 5F), the mean frequency increased by 3 kHz (control: 77.50 ± 0.08 kHz; *Agrp^{Trpv1}*: 80.96 ± 0.07 kHz; $D = 0.12$, $p = 10^{-15}$, KS test; Figure 5G), and the bandwidth increased by 2 kHz (control: 27.31 ± 0.13 kHz; *Agrp^{Trpv1}*: 29.84 ± 0.12 kHz; $D = 0.07$, $p = 10^{-15}$, KS test; Figure 5H). The selected categories of USVs induced by activation of *Agrp* neurons (Figure 5I) showed a higher complexity compared to those suppressed in *Agrp^{Vgat-KO}* mice (Figure 4).

Interestingly, when we analyzed the relative frequency of USV categories, we found a selective increase in the frequency of “chevrons” upon chemogenetic activation of *Agrp* neurons (Figures 5J and 4N). To further corroborate these findings, we used a second software tool MUPET to classify vocalizations based on their shape (Van Segbroeck et al., 2017). We found six clusters of vocalizations that showed a more than 2.5-fold increase upon activation of *Agrp* neurons (Figures 5K and 5L). These clusters were very similar to each other, resembling our previous analysis (Figures 4G and 4H). We also found that activation of *Agrp* neurons suppressed vocalizations in cluster 39 (Figures 5K and 5M). The USVs in cluster 39 were simpler in shape, resembling vocalizations predominantly emitted by *Agrp^{Vgat-KO}* pups (Figure 4). In contrast to mice lacking GABA release by *Agrp* neurons, chemogenetic activation of these neurons stimulated USV emission at a higher rate and with higher complexity. Together, these results strongly suggest a model in which neonatal *Agrp* neurons are rapidly activated upon isolation from the nest, which modulates USV emission, presumably to attract the dam.

Chemogenetic Activation of *Agrp* Neurons in Neonatal Mice Modulates the Behavior of Dams

Neonatal behavior is linked to maternal behavior, as the former can enhance and entrain the behavior of the latter. Based on our previous results, we expected that chemogenetic activation of *Agrp* neurons in the neonate would change the response of the dam toward the neonate. We devised a test to assess maternal responsiveness to P10 mice, the “maternal preference test” (Figure 5N). In this test, maternal responsiveness was measured

as the time of dam-pup interaction. We found maternal exploratory behavior was strongly skewed toward *Agrp^{Trpv1}* pups compared to controls (preference index - control: 44.96 ± 13.68 s, $n = 25$; *Agrp^{Trpv1}*: 125.1 ± 21.74 s, $n = 25$; $t_{24} = 2.69$; $p = 0.01$, 2-tailed paired *t* test; Figures 5O and 5P). These results support the model in which neonatal *Agrp* neurons modulate vocal behaviors signaling the dam should return to the nest.

Chemogenetic Activation of Neonatal *Agrp* Neurons Increases Odds for Nipple Attachment

In young pups, contact with the dam is critical for suckling behavior and ingestion of breast milk. Thus, we next devised behavior experiments to test whether activation of *Agrp* neurons in pups would drive behaviors toward the dam, including exploratory activity, suckling, and milk intake. We eliminated active participation by the dam as the driver of these behaviors by examining the behavior of P10 mice toward anesthetized dams (Figure 6A). In anesthetized dams, milk ejection decreases considerably (Lincoln et al., 1973), so suckling under these conditions is considered non-nutritive. Indeed, we did not observe the stretching reflex in pups that suckled during our experiments, which is a pathognomonic sign of milk ejection and ingestion (Vorherr et al., 1967).

Activation of *Agrp* neurons in P10 mice increased the total number of pups that attached to the dam’s nipples (control: 9 out of 22; *Agrp^{Trpv1}*: 13 out of 15; $p = 0.005$, chi-square test; Figure 6B) and increased the distance traveled in the testing chamber (control: 0.75 ± 0.14 m, $n = 22$; *Agrp^{Trpv1}*: 1.20 ± 0.21 m, $n = 15$; $U = 94$, $p = 0.027$, Mann-Whitney test; Figures 6C and 6D). We then compared nipple attachment behavior of P10 mice, excluding animals that did not attach to the dam’s nipples from post hoc analysis. Chemogenetic activation of *Agrp* neurons did not change the frequency (control: 3.11 ± 1.23 ; *Agrp^{Trpv1}*: 3.61 ± 0.83 ; $U = 51$, $p = 0.63$, Mann-Whitney test; Figure 6E), latency (control: 279.9 ± 57.4 s; *Agrp^{Trpv1}*: 485.4 ± 86.2 s; $U = 35$, $p = 0.12$, Mann-Whitney test; Figure 6F), or the duration of nipple attachment (control: 719.4 ± 128.0 s; *Agrp^{Trpv1}*: 529.8 ± 99.86 s; $U = 39$, $p = 0.20$, Mann-Whitney test; Figure 6G). Thus, while chemogenetic activation of *Agrp* neurons in P10 mice increased the probability of attaching to the dam’s nipples, it did not change the observable microstructure of nipple attachment behavior.

(D) Total number of USVs during recording from (C) (nest, $n = 3$; isolation and room temperature, $n = 16$; isolation and thermoneutrality, $n = 4$; one-way ANOVA, $p < 10^{-4}$).

(E) Tukey-Kramer’s multiple comparisons test of the difference between means (95% confidence intervals from D), representing effect sizes.

(F) The total number of vocalizations upon isolation (10 min) in *Npy^{+/+}* ($n = 12$), *Npy^{KO/+}* ($n = 17$), and *Npy^{KO/KO}* ($n = 7$) P10 mice; Kruskal-Wallis test, $p = 0.74$.

(G) Similar to (F) but using P10 mice knockout for *Vgat* specifically in *Agrp* neurons (*Agrp^{Vgat-KO}*) and their littermate controls (control, $n = 10$; *Agrp^{Vgat-KO}*, $n = 14$; Mann-Whitney test, $p < 10^{-5}$).

(H) Raster plots; ticks represent USVs. Each row represents an animal.

(I–K) Violin plots representing the distribution of USV characteristics in control ($n = 3,427$ USVs) and *Agrp^{Vgat-KO}* mice ($n = 786$ USVs) in (I) duration, (J) mean frequency of the main component, and (K) the bandwidth; p values calculated using the Kolmogorov-Smirnov test.

(L–V) Types of USVs labeled in this study. Each panel represents the spectrogram of one type of vocal call as followed: (L) Step-up, (M) Down-frequency modulation, (N) Chevron, (O) Short, (P) Flat, (Q) Two-steps, (R) Up-frequency modulation, (S) Complex, (T) Multi-steps, (U) Step-down and (V) Reverse chevron.

(X) Distribution of absolute counts of each vocal call type.

(Y) Similar to (X) but vocal types normalized to total counts. In (X) and (Y), multiple *t* tests with p values corrected for multiple comparisons using the Holm-Sidak method.

In (C), symbols represent mean \pm SEM. In (D), (F), (G), (X), and (Y), bars represent mean \pm SEM. In (E), symbols represent mean \pm 95% CI. In (I)–(K), data distribution is plotted. In (D), (F), and (G), symbols represent individual data. Statistically significant p values are displayed in the panels.

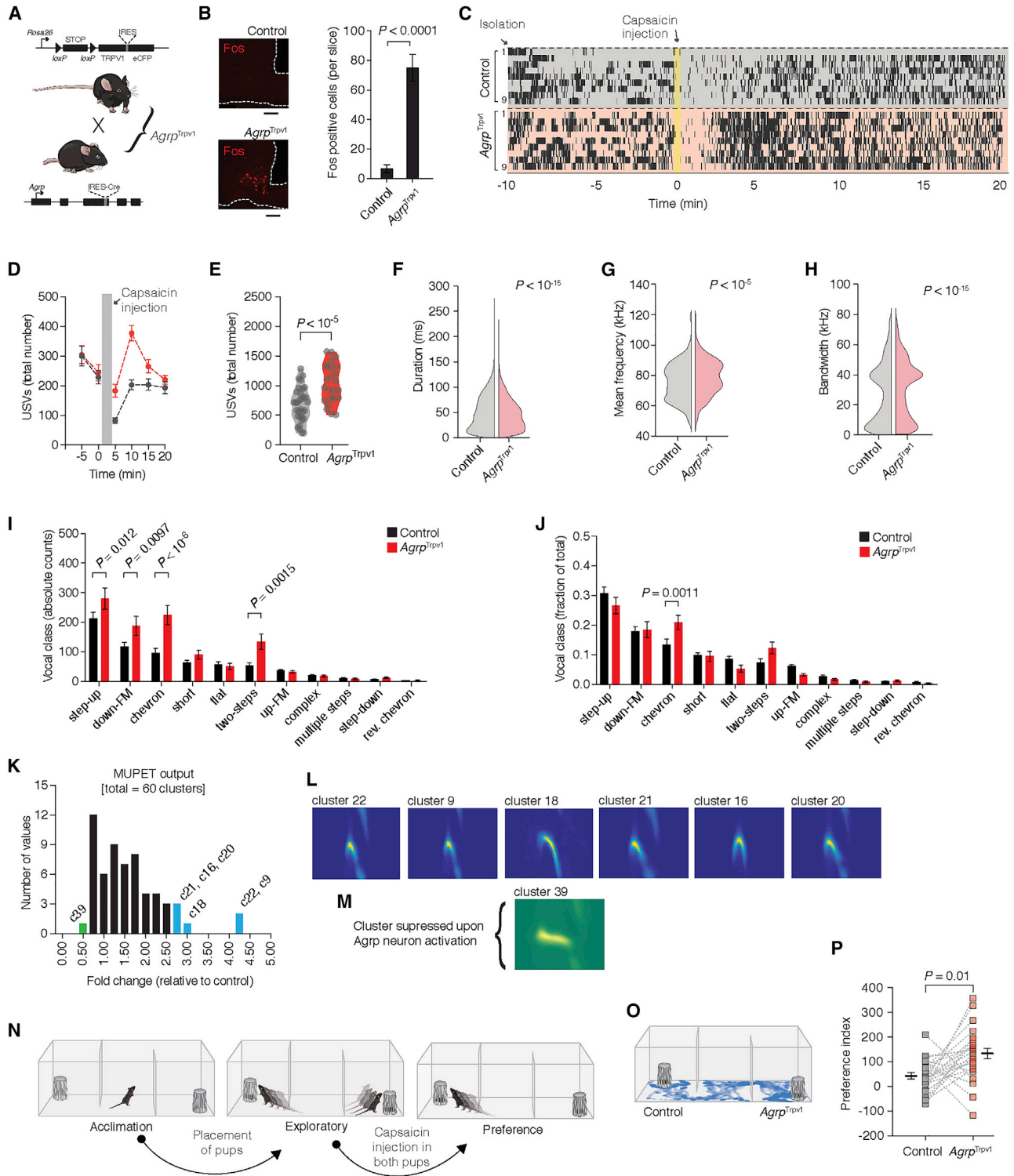


Figure 5. Activation of *Agrp* Neurons in P10 Mice Increases USV Emission and Alters the Dam's Behavior

(A) Generation of *Agrp^{Trpv1}* mice.

(B) Fos in the arcuate nucleus of P15 *Agrp^{Trpv1}* mice upon injection of capsaicin (10 mg/kg, s.c.; n = 5 mice per group). Scale bar corresponds to 50 μ m. Bars and symbols represent mean \pm SEM.

(C) Raster plots show USV in isolated P10 controls (n = 32) and *Agrp^{Trpv1}* mice (n = 24). A tick represents a USV.

(D) Related to (C), number of USVs (in 5-min bins).

(legend continued on next page)

Next, we investigated the influence of the environmental temperature on nipple attachment behavior (Figure 6H). Thermal support from underneath the testing chamber completely suppressed nipple attachment behavior in P10 control mice (0 out of 11 pups tested attached), while 4 out of 10 pups with activated *Agrp* neurons attached to the dam's nipples ($p = 0.019$, chi-square test; Figure 6I). Interestingly, the arousal response of P10 mice upon activation of *Agrp* neurons was intact, as measured by the distance traveled during the test (control: 0.30 ± 0.07 m, $n = 11$; *Agrp*^{Trpv1}: 1.03 ± 0.19 m, $n = 10$; $U = 13$, $p = 0.002$, Mann-Whitney test; Figures 6J and 6K). When we analyzed the different components of nipple attachment behavior of the four P10 mice that successfully attached, we found the frequency of attachments was largely suppressed with mice only attaching once during the test (Figure 6L). The latency to attach (386.5 ± 49.62 s; Figure 6M) was similar to the other experimental conditions (Figures 6F and 6S). The duration animals remained attached to the nipples (787.9 ± 48.20 s; Figure 6N) was within the range of our other experiments (Figures 6G and 6T). We conclude providing warmth did not blunt the arousal response after activating *Agrp* neurons but did suppress nipple attachment behavior of P10 mice. Taken together, our behavioral experiments further support the importance of a thermal stimulus in neonates to modulate the functional properties of *Agrp* neurons.

We then assessed whether a lactating anaesthetized dam would alter attachment by P10 mice. Oxytocin triggers the milk ejection reflex following nipple stimulation by the pups during suckling (Lincoln and Paisley, 1982). To facilitate milk ejection, we injected a group of anesthetized dams with oxytocin immediately before testing each pup (Figure 6O) (Singh and Hofer, 1978; Vorherr et al., 1967). Similar to non-lactating dams, activation of *Agrp* neurons in P10 mice increased the number of mice that attached to the dam's nipples (control: 8 out of 18; *Agrp*^{Trpv1}: 13 out of 15; $p = 0.012$, chi-square test; Figure 6P). The total distance traveled during the test was not different between groups (control: 0.87 ± 0.22 m, $n = 18$; *Agrp*^{Trpv1}: 1.13 ± 0.28 m, $n = 15$; $U = 100.5$, $p = 0.21$, Mann-Whitney test; Figure 6Q). When comparing the behavior of animals that attached to the dam's nipples, we did not find statistical differences in the frequency (control: 5.25 ± 0.99 , $n = 8$; *Agrp*^{Trpv1}: 8.38 ± 1.52 , $n = 13$;

$U = 34$, $p = 0.20$, Mann-Whitney test; Figure 6R) or duration of attachments (control: 515.7 ± 78.68 s, $n = 8$; *Agrp*^{Trpv1}: 502.6 ± 91.98 s, $n = 13$; $U = 50$, $p = 0.91$, Mann-Whitney test; Figure 6T), but we found a decrease in the latency of attachment (control: 501.9 ± 68.91 s, $n = 8$; *Agrp*^{Trpv1}: 335.2 ± 55.52 s, $n = 13$; $U = 21$, $p = 0.02$, Mann-Whitney test; Figure 6S). Since dams were lactating, we also measured body-weight changes in the pups as a measure of milk intake. Interestingly, upon activation of *Agrp* neurons, P10 mice ingested a lower amount of milk than controls during the test (control: 91.2 ± 19.9 mg; *Agrp*^{Trpv1}: 43.7 ± 10.0 mg; pups that did not attach: -10.0 ± 2.9 mg, $n = 12$; $F_{2,30} = 19.35$, $p < 10^{-5}$, one-way ANOVA; Figures 6U and 6V). These results suggest that activated *Agrp* neurons increase dam-seeking behavior but not necessarily increase ingestion of milk.

Chemogenetic Activation of *Agrp* Neurons Increases Ingestive Behaviors in P15 Mice

Mice rapidly transition from breastfeeding to independent feeding during weaning period. At approximately P15, mice begin experimenting with food sources but still rely on breastfeeding for nutrition (Hammond et al., 1996). We next examined the behavior of P15 mice toward the dam to investigate the ontogeny of *Agrp* neuron function. All tested P15 mice attached to the nipples of the anesthetized dam regardless of chemogenetic activation of *Agrp* neurons ($n = 19$ mice per group; Figure 7A). Activating *Agrp* neurons did not significantly change the distance traveled in the testing chamber (control: 2.03 ± 0.34 m; *Agrp*^{Trpv1}: 2.20 ± 0.22 m; $U = 145$, $p = 0.31$, Mann-Whitney test; Figure 7B). In contrast to P10 mice, chemogenetic activation of *Agrp* neurons in P15 mice showed a striking increase in the number of attachments to the dam's nipples compared to control (control: 3.68 ± 1.02 ; *Agrp*^{Trpv1}: 11.74 ± 1.80 ; $U = 72.5$, $p = 0.001$; Mann-Whitney test; Figures 7C and 7D). We observed no statistical difference in the latency of the first attachment (control: 226.6 ± 50.8 s; *Agrp*^{Trpv1}: 123.0 ± 16.92 s; $U = 116$, $p = 0.06$; Mann-Whitney test; Figure 7E) or the total duration of nipple attachment (control: 711.6 ± 85.2 s; *Agrp*^{Trpv1}: 798.9 ± 79.02 s; $U = 143$, $p = 0.28$; Mann-Whitney test; Figure 7F).

Since P15 mice displayed numerous nipple attachments (Figure 7D), we could track and quantify the number of nipples

(E) Related to (C) and (D), total number of USVs in the 20 min after activating *Agrp* neurons in isolated pups (control, $n = 32$; *Agrp*^{Trpv1}, $n = 24$; p value calculated using a 2-tailed unpaired t test).

(F–H) Violin plots representing the distribution of USV characteristics in control ($n = 22,168$ USVs) and *Agrp*^{Trpv1} mice ($n = 24,971$ USVs) in (F) duration, (G) mean frequency of the main component of the USV, and (H) the bandwidth; p values calculated using the Kolmogorov-Smirnov test.

(I) Distribution of absolute counts of each vocal call type.

(J) Similar to (I), but vocal types normalized to total counts. In (I) and (J), multiple t tests with p values corrected for multiple comparisons using the Holm-Sidak method.

(K) Distribution of the fold change (number of USVs from *Agrp*^{Trpv1} mice related to number of USVs from control mice) in each of the 60 output clusters analyzed by MUPET (see STAR Methods). Shown in blue are 6 clusters highly enriched in USVs from *Agrp*^{Trpv1} mice. Shown in green is 1 cluster enriched in USVs from controls.

(L) Related to (K), images represent the 6 clusters enriched in USVs from *Agrp*^{Trpv1} mice.

(M) Related to (K), image represents the cluster enriched in USVs from control mice.

(N) Maternal preference test (MPT).

(O) Representative tracking (in blue) of a dam in the preference stage.

(P) Preference index (in seconds) during MPT ($n = 25$ pairs; p value calculated using a 2-tailed paired t test).

In (D), symbols represent mean \pm SEM. In (B), (I), and (J), bars represent mean \pm SEM. In (F)–(H), data distribution is plotted. In (E) and (P), symbols represent individual data. In (P), black lines indicate mean \pm SEM. See also Figure S1.

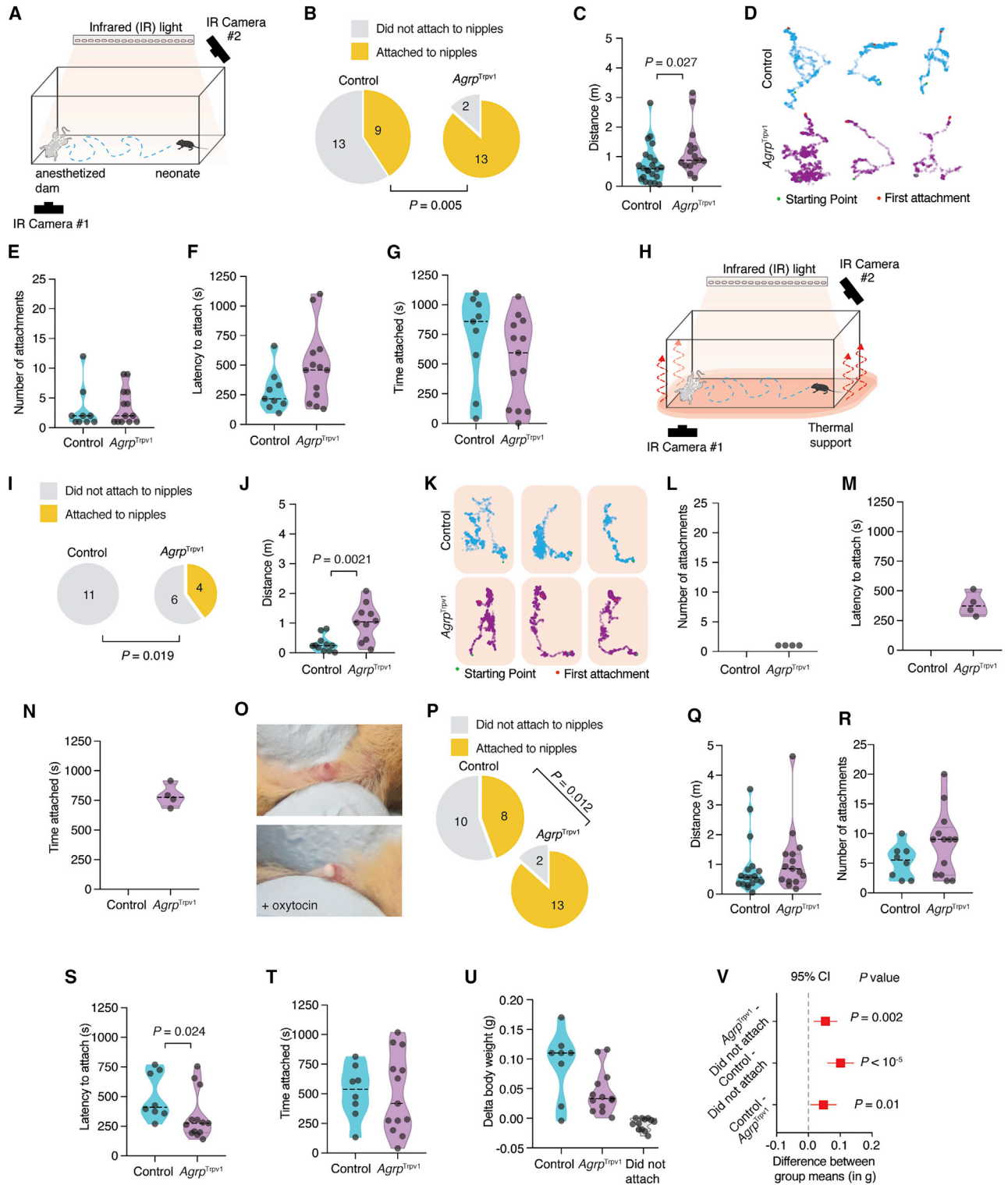


Figure 6. Agrp Neuron Activation and Suckling Behavior in P10 Mice

(A) Chamber to assay suckling behavior in mice.

(B–G) Quantification of suckling behavior in P10 mice tested with an anesthetized, non-lactating dam. In (B), proportion of mice displaying nipple attachment. In (C), total distance traveled. In (D), tracking of locomotor activity (bottom: starting point; top: anesthetized dam). In (E)–(G), data only considering mice that attached to nipples. In (E), number of nipple attachments. In (F), latency to the first attachment. In (G), total time attached to nipples.

(legend continued on next page)

explored to measure nipple-shifting behavior (Figure 7G) (Cramer et al., 1980). Chemogenetic activation of *Agrp* neurons in P15 mice increased the total number of different nipples explored during the test (control: 2.68 ± 0.57 nipples; *Agrp*^{Trpv1}: 5.21 ± 0.62 nipples; $U = 92.5$, $p = 0.007$; Mann-Whitney test; Figure 7H). In these experiments, mice did not show a nipple preference ($n = 38$ mice; $p = 0.42$, one-way ANOVA; Figures 7I and 7J), which is a phenomenon observed in other species (Erwin et al., 1975; Hudson et al., 2009; Tomaszycy et al., 1998).

We repeated the above experiments using anesthetized dams injected with oxytocin during a 10-min test. In control mice, 50% of P15 mice attached to the dam's nipples (4 out of 8 mice), while 91% of *Agrp*^{Trpv1} mice displayed the same behavior (11 out of 12 mice; $p = 0.035$, chi-square test; Figure 7K). Activating *Agrp* neurons did not significantly change the distance traveled in the testing chamber (control: 1.13 ± 0.26 m; *Agrp*^{Trpv1}: 1.56 ± 0.21 m; $U = 31$, $p = 0.20$, Mann-Whitney test; Figure 7L) but strongly increased the number of nipple attachments (control: 2.00 ± 0.70 ; *Agrp*^{Trpv1}: 9.90 ± 1.82 ; $U = 2.5$, $p = 0.007$, Mann-Whitney test; Figure 7M). The latency to the first nipple attachment (control: 162.0 ± 33.1 s; *Agrp*^{Trpv1}: 119.9 ± 27.1 s; $U = 14$, $p = 0.34$, Mann-Whitney test; Figure 7N) and the total duration of nipple attachment (control: 332.2 ± 11.9 s; *Agrp*^{Trpv1}: 388.0 ± 34.7 s; $U = 20$, $p = 0.85$, Mann-Whitney test; Figure 7O) were not changed upon chemogenetic activation of *Agrp* neurons. In contrast to P10 mice, chemogenetic activation of *Agrp* neurons in P15 mice did significantly increase milk intake in mice that attached to the nipples of lactating dams (control: 17.2 ± 26.1 mg; *Agrp*^{Trpv1}: 109.5 ± 38.7 mg; $U = 7$, $p = 0.02$, Mann-Whitney test; Figure 7P).

We also tested the extent to which activation of *Agrp* neurons induces ingestion of solid food during the weaning period. We did not observe changes in food intake in P15 mice, but we observed increased food intake in P18 and P21 mice upon chemogenetic activation of *Agrp* neurons (Figure 7Q). Similarly, we only found changes in body weight during the feeding test in P21 mice (Figure 7R). Together, this set of behavioral experiments suggest that *Agrp* neurons in P10 mice are not proximally involved in milk intake or signaling milk ingestion. We propose that these functional properties of *Agrp* neurons rapidly change (or appear) as mice approach weaning age.

DISCUSSION

Overall, our results reveal functional properties of *Agrp* neurons in neonatal mice. These insights demonstrate developmental differences that emerge during ontogeny, so studying any complex system may remain incomplete without assessing its developmental properties (Tinbergen, 1963).

Our experiments unexpectedly revealed that *Agrp* neurons are functional during the first 2 postnatal weeks in mice despite their immature characteristics (Nilsson et al., 2005; Padilla et al., 2010). We showed that *Agrp* neurons in P10 mice did not respond to milk intake and their activation did not directly increase milk intake. Conversely, non-nutritive suckling and thermal insulation were key factors modulating the activity of *Agrp* neurons. These results are compatible with the physiology of breastfeeding in neonatal mammals. During breastfeeding, mice, like most other mammals, do not receive continuous milk ejection. Milk ejection remains under control of a neuroendocrine reflex (Cross and Harris, 1952) and occurs at random intervals, as demonstrated in rats (Lincoln et al., 1973). In spite of milk ejection patterns, neonatal rats stay attached to the dam's nipple for at least 12 h a day in the first days of life (Lincoln et al., 1973). In fact, homeostatic sensing of milk deprivation to modulate nutritive suckling behavior only develops later as shown in laboratory rodents (Ellis et al., 1984; Hall and Rosenblatt, 1978; Kenny et al., 1979). Thus, these studies strongly imply that nipple attachment serves as a stimulus for more than milk ejection. In fact, neonatal rodents develop filial huddling to dams triggered by thermo-tactile stimulation rather than provision of milk (Alberts, 2007; Alberts and May, 1984). Similar to rodents, neonatal monkeys prefer a cloth mother that provides thermal and tactile stimuli to a wired mother with a nursing bottle (Harlow, 1958), establishing that maternal comfort has a superior importance compared to milk intake in driving neonatal affectional responses. We posit that *Agrp* neurons of neonates drive this milk-independent encoding of the offspring-to-caregiver bond.

In our studies, thermal insulation was the primary factor modulating the activation of *Agrp* neurons in neonates following isolation from the nest. Notably, experiencing previous thermal challenges was not significant to activate neonatal *Agrp* neurons following isolation from the nest, which suggests an "innate" property of *Agrp* neurons. Intriguingly, foster dams also provide thermal insulation for the neonates, but they do not suppress activation of *Agrp* neurons after isolation from

(H) Suckling behavior using thermal support ($\approx 35^\circ\text{C}$).

(I–N) Quantification of suckling behavior in P10 mice tested with an anesthetized, non-lactating dam (as displayed in H). In (I), proportion of mice that attached to the nipples. In (J), total distance traveled. In (K), tracking of locomotor activity (bottom: starting point; top: anesthetized dam). In (L), number of nipple attachments. In (M), latency to the first attachment. In (N), total time attached to nipples.

(O) Milk letdown prior to and after oxytocin injection in anesthetized dams.

(P–T) Quantification of suckling behavior in P10 mice tested with an anesthetized, lactating dam. In (P), proportion of P10 mice that attached to the nipples. In (Q), total distance traveled. In (R)–(T), data only reflect pups that attached to nipples. In (R), number of nipple attachments. In (S), latency to the first attachment. In (T), the total time attached to nipples.

(U) Delta body weight after suckling assay (control, $n = 8$; *Agrp*^{Trpv1}, $n = 13$; pups that did not attach, $n = 12$; one-way ANOVA, $p < 10^{-5}$).

(V) Tukey-Kramer's multiple comparisons test of the difference between means (95% confidence intervals from U), representing effect sizes.

In (B), (I), and (P), statistical analysis was performed using the chi-square test (2-tailed). In yellow, proportion of mice that attached to the dam's nipples are shown. In gray, mice that did not attach are shown.

In (C), (E)–(G), (J), (L)–(N), and (Q)–(U), violin plots represent the distribution of the data. Symbols represent individual values. Statistical analysis was performed using Mann-Whitney test, with the exception of (U). p values are provided in the panels when statistically significant.

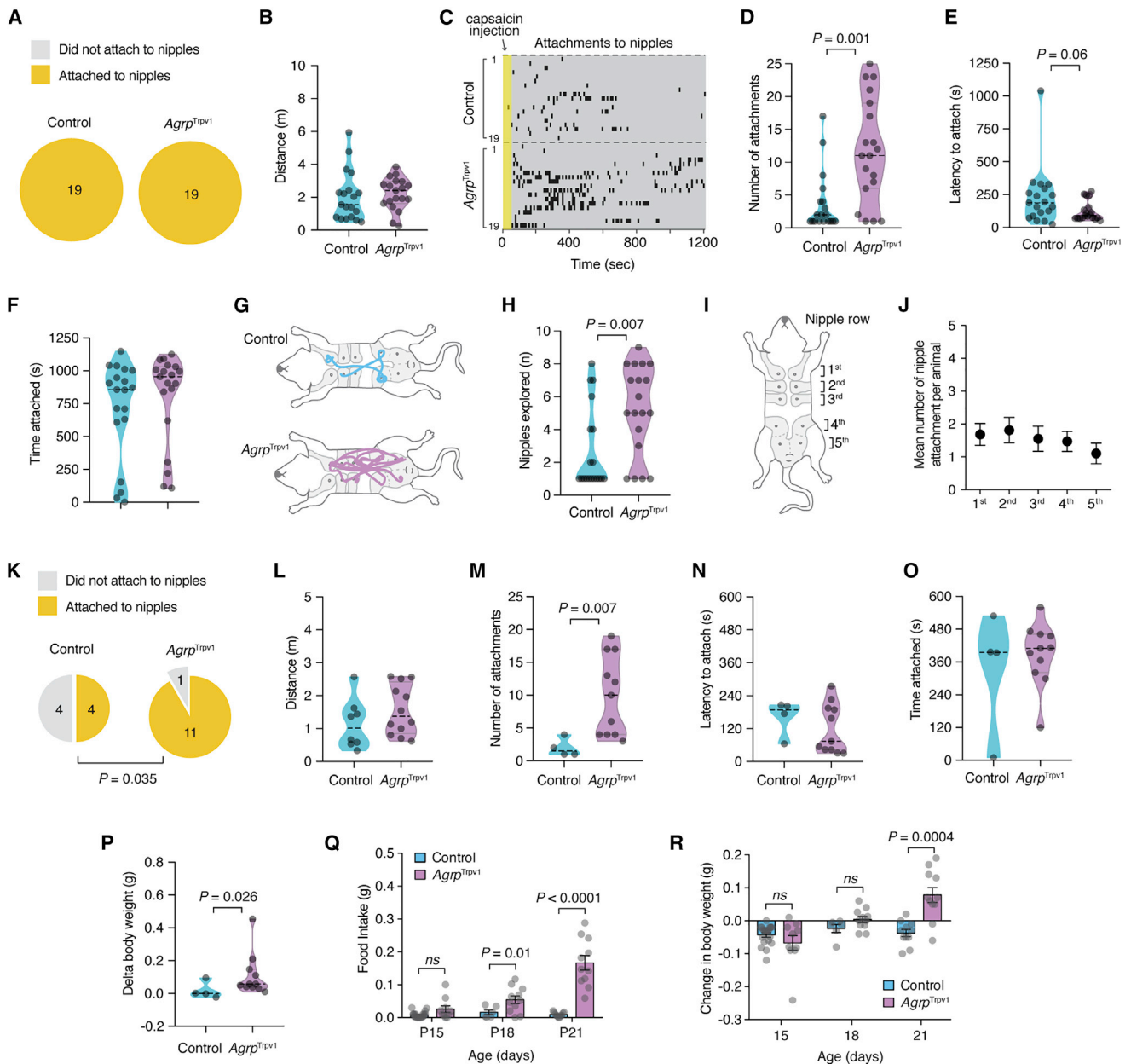


Figure 7. Ontogeny of Ingestive Behaviors in Mice

(A–J) Suckling behavior in P15 mice using anesthetized non-lactating dams during a 20-min test. (A) All pups attached to the dam's nipples during the test. (B) Total distance traveled. (C) Raster plot, ticks indicate nipple attachment. (D) Number of nipple attachments. (E) Latency to the first nipple attachment. (F) Total time attached to nipples. (G) Representative tracking data of nipple attachment. (H) Number of nipples explored. (I) Illustration of the location and number of nipples in the dam and (J) nipple preference as measured by the number of nipple attachments per nipple row in P15 mice ($n = 38$; both control and *Agrp*^{Trpv1} mice were included).

(K–O) Suckling behavior in P15 mice using anesthetized lactating dams during a 10-min test. (K) Proportion of P15 mice that attached to the nipples of lactating dams. In (L), total distance traveled during the test. In (M)–(O), only showing mice that attached to nipples. In (M), the number of nipple attachments is shown. In (N), latency to the first attachment is shown. In (O), total time attached to nipples is shown.

(P) Delta body weight after the suckling assay (control, $n = 4$; *Agrp*^{Trpv1} $n = 11$).

(Q) Chow intake during 30 min after activation of *Agrp* neurons in mice at 15, 18, and 21 days of age.

(R) Delta body weight in the same animals as in (Q).

In (A) and (K), statistical analysis performed using the chi-square test (2-tailed). In yellow, proportion of mice that attached to the dam's nipples. In gray, mice that did not attach. In (B), (D)–(F), (H), and (L)–(P), violin plots represent the distribution of the data. Symbols represent individual values. Statistical analysis performed using Mann-Whitney test. In (Q) and (R), differences tested using unpaired t test with Welch's correction (unequal SDs) are shown. p values provided in the panels when statistically significant. Bars and symbols (in J, Q, and R) represent mean \pm SEM.

the nest to the same degree as thermal support. This observation suggests that neonates integrate several sensory signatures coupled to the nest environment, such as sensory cues from the dam, siblings, home-nest odors, or from all these sources, to create and build expectations of the external world. We unexpectedly propose that activity of *Agrp* neurons partially encodes this information. Future studies should address the exact nature of this information and the combination of sensory modalities needed to modulate the activity of neonatal *Agrp* neurons.

Our results provide further evidence to the proposal that *Agrp* neurons serve as motivational drivers in the mammalian brain. In adult mice, *Agrp* neurons may encode negative valence (Betley et al., 2015). Under this proposal, these neurons when active would generate an unpleasant state of hunger leading the adult mouse to engage in behaviors to eat and suppress this state (Betley et al., 2015). Our results support this functional property of *Agrp* neurons in encoding an overall negative state beginning in early development. Clearly, isolation from the nursing nest serves as a negative stimulus for the neonate, which triggers a rapid activation of *Agrp* neurons and emission of vocalizations. Conversely, reunion then serves as a positive stimulus for the isolated neonate, which immediately suppresses the activity of *Agrp* neurons. By studying the functional ontogeny of *Agrp* neurons, our results support a model by which *Agrp* neurons generate a motivational drive to suppress an overall negative state.

In our studies, we could not find increases in corticosterone levels upon isolation or an enhanced activation of *Agrp* neurons (as labeled by Fos) in the presence of predator odor. Despite these negative results, we cannot rule out the possibility that *Agrp* neurons early in life are responsive to general stressors.

Upon parental separation, some infant mammals and birds respond with protest, despair, and emit sounds to attract them (Hofer, 1994). Our results demonstrated that neonatal *Agrp* neurons are a critical component of the circuit modulating vocal behavioral response in mice. These findings provide further insight into the underlying neural pathways subserving neonatal vocal behavior (Curry et al., 2013; Mosienko et al., 2015; Winslow et al., 2000). Investigating downstream circuits linking *Agrp* neurons to brain regions involved in the emission of USVs (Arriaga and Jarvis, 2013; Arriaga et al., 2012) will reveal how the neonatal brain encodes sensory information and internal state-dependent variables to generate behavioral responses (Boulanger-Bertolus et al., 2017; Hofer, 1996).

Our results have a broad impact to understand the functional ontogeny of hypothalamic neurons and the importance of the neonatal period in brain and behavior development. Additionally, these studies establish a mechanistic substrate underlying infant-caregiver interaction, which suggests an initial population of neurons underlying the long-sought nature of this social bond in mammals (Harlow, 1958; Lewis et al., 2007).

STAR★METHODS

Detailed methods are provided in the online version of this paper and include the following:

- **KEY RESOURCES TABLE**
- **CONTACT FOR REAGENT AND RESOURCE SHARING**
- **EXPERIMENTAL MODELS AND SUBJECT DETAILS**
- **METHOD DETAILS**
 - Drugs
 - Immunohistochemistry
 - Isolation from the nest (Figures 1A–1D):
 - Milk intake in the nursing nest (Figures 1E and 1F):
 - Measurement of corticosterone levels (Figure 1G):
 - Isolation from the nest in the presence of a predator odor (Figures 1H–1J):
 - Isolation from the nest with milk infusion (Figures 1K–1O):
 - Mouse milk collection
 - Artificial feeding protocol (Figures 1P–1R):
 - Assessment of maternal components with foster dams (Figures 2A–2C):
 - Isolation from the nest with thermal support (Figures 2D–2G):
 - Isolation from the nest in pups raised at thermoneutrality (Figures 2H–2J):
 - Fiber photometry (Figure 3):
 - Recording of ultrasonic vocalizations (Figures 4 and 5):
 - Maternal preference test (Figures 5N–5P):
 - Analysis of ultrasonic vocalizations
 - Mouse pup behavior toward the anesthetized dam (Figures 6A–6G and 7A–7J):
 - Mouse pup behavior toward the anesthetized dams injected with oxytocin (Figures 6P–6V and 7K–7P):
 - Independent feeding (Figures 7Q and 7R):
- **QUANTIFICATION AND STATISTICAL ANALYSIS**

ACKNOWLEDGMENTS

We thank Jeremy Bober for technical support. We thank lab members as well as Dr. Ruslan Medzhitov, Dr. Ivan de Araujo, and Dr. Esther Florsheim for critical insights in the manuscript. M.O.D. was supported by a NARSAD Young Investigator Grant ID 22709 from the Brain & Behavior Research Foundation, by the National Institute of Diabetes and Digestive and Kidney Diseases of the NIH (R01DK107916), by a pilot grant from the Yale Diabetes Research Center (P30 DK045735), by the Yale Center for Clinical Investigation Scholar Award, by the Whitehall Foundation, by the Charles H. Hood Foundation, Inc. (Boston, MA), and by a pilot grant from the Modern Diet and Physiology Research Center (The John B. Pierce Laboratory). M.O.D. also received support from the Conselho Nacional de Desenvolvimento Científico e Tecnológico (CNPq) and Coordenadoria de Aperfeiçoamento de Pessoal de Nível Superior (CAPES), Brazil. M.R.Z., A.H.O.F., and R.D.P. were partially supported by scholarships from CNPq and CAPES. We thank Life Science Editors for editorial assistance.

AUTHOR CONTRIBUTIONS

M.R.Z. performed the experiments, designed the studies, analyzed the data, and helped write the manuscript. A.H.O.F. developed a tool for ultrasonic vocalization analysis in neonates and analyzed the data. R.D.P. performed part of the Fos and behavior experiments. O.I. performed the fiber photometry experiment. M.O.D. supervised the work, designed the studies, analyzed the data, and wrote the manuscript.

DECLARATION OF INTERESTS

The authors declare no competing interests.

Received: January 22, 2019

Revised: March 25, 2019

Accepted: April 12, 2019

Published: May 16, 2019

REFERENCES

- Alberts, J.R. (2007). Huddling by rat pups: ontogeny of individual and group behavior. *Dev. Psychobiol.* *49*, 22–32.
- Alberts, J.R., and May, B. (1984). Nonnutritive, thermotactile induction of filial huddling in rat pups. *Dev. Psychobiol.* *17*, 161–181.
- Arenkiel, B.R., Klein, M.E., Davison, I.G., Katz, L.C., and Ehlers, M.D. (2008). Genetic control of neuronal activity in mice conditionally expressing TRPV1. *Nat. Methods* *5*, 299–302.
- Arriaga, G., and Jarvis, E.D. (2013). Mouse vocal communication system: are ultrasounds learned or innate? *Brain Lang.* *124*, 96–116.
- Arriaga, G., Zhou, E.P., and Jarvis, E.D. (2012). Of mice, birds, and men: the mouse ultrasonic song system has some features similar to humans and song-learning birds. *PLoS ONE* *7*, e46610.
- Barros, V.N., Mundim, M., Galindo, L.T., Bittencourt, S., Porcionatto, M., and Mello, L.E. (2015). The pattern of c-Fos expression and its refractory period in the brain of rats and monkeys. *Front. Cell. Neurosci.* *9*, 72.
- Betley, J.N., Xu, S., Cao, Z.F.H., Gong, R., Magnus, C.J., Yu, Y., and Sternson, S.M. (2015). Neurons for hunger and thirst transmit a negative-valence teaching signal. *Nature* *521*, 180–185.
- Boulanger-Bertolus, J., Rincón-Cortés, M., Sullivan, R.M., and Mouly, A.M. (2017). Understanding pup affective state through ethologically significant ultrasonic vocalization frequency. *Sci. Rep.* *7*, 13483.
- Cramer, C.P., Blass, E.M., and Hall, W.G. (1980). The ontogeny of nipple-shifting behavior in albino rats: mechanisms of control and possible significance. *Dev. Psychobiol.* *13*, 165–180.
- Cross, B.A., and Harris, G.W. (1952). The role of the neurohypophysis in the milk-ejection reflex. *J. Endocrinol.* *8*, 148–161.
- Curry, T., Egeto, P., Wang, H., Podnos, A., Wasserman, D., and Yeomans, J. (2013). Dopamine receptor D2 deficiency reduces mouse pup ultrasonic vocalizations and maternal responsiveness. *Genes Brain Behav.* *12*, 397–404.
- Dana, H., Sun, Y., Mohar, B., Hulse, B., Hasseman, J.P., Tsegaye, G., Tsang, A., Wong, A., Patel, R., Macklin, J.J., et al. (2018). High-performance GFP-based calcium indicators for imaging activity in neuronal populations and microcompartments. *bioRxiv*. <https://doi.org/10.1101/434589>.
- Dietrich, M.O., Bober, J., Ferreira, J.G., Tellez, L.A., Mineur, Y.S., Souza, D.O., Gao, X.B., Picciotto, M.R., Araújo, I., Liu, Z.W., and Horvath, T.L. (2012). AgRP neurons regulate development of dopamine neuronal plasticity and nonfood-associated behaviors. *Nat. Neurosci.* *15*, 1108–1110.
- Dietrich, M.O., Zimmer, M.R., Bober, J., and Horvath, T.L. (2015). Hypothalamic AgRP neurons drive stereotypic behaviors beyond feeding. *Cell* *160*, 1222–1232.
- Ellis, S., Axt, K., and Epstein, A.N. (1984). The arousal of ingestive behaviors by chemical injection into the brain of the suckling rat. *J. Neurosci.* *4*, 945–955.
- Erwin, J., Anderson, B., and Bunger, D. (1975). Nursing behavior of infant pigtail monkeys (*Macaca nemestrina*): preferences for nipples. *Percept. Mot. Skills* *40*, 592–594.
- Girish, V., and Vijayalakshmi, A. (2004). Affordable image analysis using NIH Image/ImageJ. *Indian J. Cancer* *41*, 47.
- Görs, S., Kucia, M., Langhammer, M., Junghans, P., and Metges, C.C. (2009). Technical note: Milk composition in mice—methodological aspects and effects of mouse strain and lactation day. *J. Dairy Sci.* *92*, 632–637.
- Grimsley, J.M., Monaghan, J.J., and Wenstrup, J.J. (2011). Development of social vocalizations in mice. *PLoS ONE* *6*, e17460.
- Gropp, E., Shanabrough, M., Borok, E., Xu, A.W., Janoschek, R., Buch, T., Plum, L., Balthasar, N., Hampel, B., Waisman, A., et al. (2005). Agouti-related peptide-expressing neurons are mandatory for feeding. *Nat. Neurosci.* *8*, 1289–1291.
- Grove, K.L., and Smith, M.S. (2003). Ontogeny of the hypothalamic neuropeptide Y system. *Physiol. Behav.* *79*, 47–63.
- Güler, A.D., Rainwater, A., Parker, J.G., Jones, G.L., Argilli, E., Arenkiel, B.R., Ehlers, M.D., Bonci, A., Zweifel, L.S., and Palmiter, R.D. (2012). Transient activation of specific neurons in mice by selective expression of the capsaicin receptor. *Nat. Commun.* *3*, 746.
- Hahn, T.M., Breininger, J.F., Baskin, D.G., and Schwartz, M.W. (1998). Coexpression of AgRP and NPY in fasting-activated hypothalamic neurons. *Nat. Neurosci.* *1*, 271–272.
- Hall, W.G., and Rosenblatt, J.S. (1978). Development of nutritional control of food intake in suckling rat pups. *Behav. Biol.* *24*, 413–427.
- Hammond, K.A., Lloyd, K.C., and Diamond, J. (1996). Is mammary output capacity limiting to lactational performance in mice? *J. Exp. Biol.* *199*, 337–349.
- Harlow, H.F. (1958). The nature of love. *Am. Psychol.* *13*, 673–685.
- Hofer, M.A. (1994). Hidden regulators in attachment, separation, and loss. *Monogr. Soc. Res. Child Dev.* *59*, 192–207.
- Hofer, M.A. (1996). Multiple regulators of ultrasonic vocalization in the infant rat. *Psychoneuroendocrinology* *21*, 203–217.
- Horvath, T.L., Bechmann, I., Naftolin, F., Kalra, S.P., and Leranth, C. (1997). Heterogeneity in the neuropeptide Y-containing neurons of the rat arcuate nucleus: GABAergic and non-GABAergic subpopulations. *Brain Res.* *756*, 283–286.
- Hudson, R., Raihani, G., González, D., Bautista, A., and Distel, H. (2009). Nipple preference and contests in suckling kittens of the domestic cat are unrelated to presumed nipple quality. *Dev. Psychobiol.* *51*, 322–332.
- Joly-Amado, A., Denis, R.G., Castel, J., Lacombe, A., Cansell, C., Rouch, C., Kassir, N., Dairou, J., Cani, P.D., Ventura-Clapier, R., et al. (2012). Hypothalamic AgRP-neurons control peripheral substrate utilization and nutrient partitioning. *EMBO J.* *31*, 4276–4288.
- Kenny, J.T., Stoloff, M.L., Bruno, J.P., and Blass, E.M. (1979). Ontogeny of preference for nutritive over nonnutritive suckling in albino rats. *J. Comp. Physiol. Psychol.* *93*, 752–759.
- Lewis, T., Amini, F., and Lannon, R. (2007). *A General Theory of Love* (Knopf Doubleday Publishing Group).
- Lincoln, D.W., and Paisley, A.C. (1982). Neuroendocrine control of milk ejection. *J. Reprod. Fertil.* *65*, 571–586.
- Lincoln, D.W., Hill, A., and Wakerley, J.B. (1973). The milk-ejection reflex of the rat: an intermittent function not abolished by surgical levels of anaesthesia. *J. Endocrinol.* *57*, 459–476.
- Luquet, S., Perez, F.A., Hnasko, T.S., and Palmiter, R.D. (2005). NPY/AgRP neurons are essential for feeding in adult mice but can be ablated in neonates. *Science* *310*, 683–685.
- Mosienko, V., Beis, D., Alenina, N., and Wöhr, M. (2015). Reduced isolation-induced pup ultrasonic communication in mouse pups lacking brain serotonin. *Mol. Autism* *6*, 13.
- Nilsson, I., Johansen, J.E., Schalling, M., Hökfelt, T., and Fetissov, S.O. (2005). Maturation of the hypothalamic arcuate agouti-related protein system during postnatal development in the mouse. *Brain Res. Dev. Brain Res.* *155*, 147–154.
- Noirot, E. (1966). Ultra-sounds in young rodents. I. Changes with age in albino mice. *Anim. Behav.* *14*, 459–462.
- Noirot, E. (1968). Ultrasounds in young rodents. II. Changes with age in albino rats. *Anim. Behav.* *16*, 129–134.
- Padilla, S.L., Carmody, J.S., and Zeltser, L.M. (2010). Pomc-expressing progenitors give rise to antagonistic neuronal populations in hypothalamic feeding circuits. *Nat. Med.* *16*, 403–405.

- Ruan, H.B., Dietrich, M.O., Liu, Z.W., Zimmer, M.R., Li, M.D., Singh, J.P., Zhang, K., Yin, R., Wu, J., Horvath, T.L., and Yang, X. (2014). O-GlcNAc transferase enables AgRP neurons to suppress browning of white fat. *Cell* 159, 306–317.
- Schindelin, J., Arganda-Carreras, I., Frise, E., Kaynig, V., Longair, M., Pietzsch, T., Preibisch, S., Rueden, C., Saalfeld, S., Schmid, B., et al. (2012). Fiji: an open-source platform for biological-image analysis. *Nat. Methods* 9, 676–682.
- Singh, P.J., and Hofer, M.A. (1978). Oxytocin reinstates maternal olfactory cues for nipple orientation and attachment in rat pups. *Physiol. Behav.* 20, 385–389.
- Takahashi, K.A., and Cone, R.D. (2005). Fasting induces a large, leptin-dependent increase in the intrinsic action potential frequency of orexigenic arcuate nucleus neuropeptide Y/Agouti-related protein neurons. *Endocrinology* 146, 1043–1047.
- Tinbergen, N. (1963). On aims and methods of Ethology. *Z. Tierpsychol.* 20, 410–433.
- Tomaszycki, M., Cline, C., Griffin, B., Maestriperri, D., and Hopkins, W.D. (1998). Maternal cradling and infant nipple preferences in rhesus monkeys (*Macaca mulatta*). *Dev. Psychobiol.* 32, 305–312.
- Van Segbroeck, M., Knoll, A.T., Levitt, P., and Narayanan, S. (2017). MUPET-Mouse Ultrasonic Profile ExTraction: A Signal Processing Tool for Rapid and Unsupervised Analysis of Ultrasonic Vocalizations. *Neuron* 94, 465–485.
- Vorherr, H., Kleeman, C.R., and Lehman, E. (1967). Oxytocin-induced stretch reaction in suckling mice and rats: a semiquantitative bio-assay for oxytocin. *Endocrinology* 81, 711–715.
- Winslow, J.T., Hearn, E.F., Ferguson, J., Young, L.J., Matzuk, M.M., and Insel, T.R. (2000). Infant vocalization, adult aggression, and fear behavior of an oxytocin null mutant mouse. *Horm. Behav.* 37, 145–155.
- Zippelius, H.-M., and Schleidt, W.M. (1956). Ultraschall-Laute bei jungen Mäusen. *Naturwissenschaften* 43, 502.

STAR★METHODS

KEY RESOURCES TABLE

REAGENT or RESOURCE	SOURCE	IDENTIFIER
Antibodies		
Rabbit polyclonal anti-c-Fos	Santa Cruz Biotechnologies	Cat# sc-52-G; RRID: AB_2629503
Rabbit monoclonal anti-c-Fos (9F6)	Cell Signaling Technology	Cat# 2250; RRID: AB_2247211
Mouse polyclonal anti-HA	BioLegend	Cat# 901503; RRID: AB_2565005
Donkey anti-mouse IgG (H+L), Alexa Fluor 488	Thermo Fisher Scientific	Cat# A-21202; RRID: AB_141607
Donkey anti-rabbit IgG (H+L), Alexa Fluor 594	Thermo Fisher Scientific	Cat# A-21207; RRID: AB_141637
Donkey anti-rabbit IgG (H+L), Alexa Fluor 647	Thermo Fisher Scientific	Cat# A-31573; RRID: AB_2536183
Bacterial and Virus Strains		
AAV8-CAG-Flex-jGCaMP7s-WPRE-SV40	Janelia Research Campus	Addgene, 104495
Biological Samples		
N/A		
Chemicals, Peptides, and Recombinant Proteins		
Capsaicin	Sigma-Aldrich	Cat# M2028-1G
Oxytocin	Sigma-Aldrich	Cat# O4375-250IU
Critical Commercial Assays		
Corticosterone ELISA kit	Enzo Life Sciences	ADI-900-097
Deposited Data		
N/A		
Experimental Models: Cell Lines		
N/A		
Experimental Models: Organisms/Strains		
Mouse: <i>Agrp</i> ^{Cre} , <i>AgRPtm1(cre)Lowl/J</i>	The Jackson Laboratory	JAX: 012899
Mouse: <i>R26</i> ^{L^{SL}-Trpv1} , B6;129P2-Gt(ROSA)26Sortm1(Trpv1,ECFP)Mde/J	The Jackson Laboratory	JAX: 008513
Mouse: <i>Trpv1</i> ^{KO} , B6.129X1-Trpv1tm1Jul/J	The Jackson Laboratory	JAX: 003770
Mouse: <i>Rpl22</i> ^{L^{SL}-HA} , B6N.129-Rpl22tm11Psam/J	The Jackson Laboratory	JAX: 011029
Mouse: <i>Npy</i> ^{KO} , 129S- <i>Npy</i> ^{tm1Rpa/J}	The Jackson Laboratory	JAX: 004545
Mouse: <i>Vgat</i> ^{Flox/Flox} , <i>Slc32a1</i> ^{tm1Lowl}	The Jackson Laboratory	JAX: 012897
Oligonucleotides		
Trpv1 knockout Wild type (5'-TGGCTCATATTTG CCTTCAG-3')	Yale Keck Oligonucleotide Synthesis	Custom preparation
Trpv1 knockout Common (5'-CAGCCCTAGGAG TTGATGGA-3')	Yale Keck Oligonucleotide Synthesis	Custom preparation
Trpv1 knockout Mutant (5'-TAAAGCGCATGCTC CAGACT-3')	Yale Keck Oligonucleotide Synthesis	Custom preparation
Ectopic Trpv1 allele F (5'-TCCCAAAGTCGCTC TGAGTT-3')	Yale Keck Oligonucleotide Synthesis	Custom preparation
Ectopic Trpv1 ectopic (5'-TGGCTTGAGTTAG GGTCTC-3')	Yale Keck Oligonucleotide Synthesis	Custom preparation
Recombinant DNA		
N/A		
Software and Algorithms		
ImageJ/Fiji	Girish and Vijayalakshmi, 2004; Schindelin et al., 2012	https://imagej.nih.gov/ij/ , RRID:SCR_002285
MUPET	Van Segbroeck et al., 2017	https://sail.usc.edu/mupet

(Continued on next page)

Continued

REAGENT or RESOURCE	SOURCE	IDENTIFIER
Any-Maze	Stoelting Co	http://www.anymaze.co.uk/index.htm , RRID:SCR_014289
GraphPad Prism 8.0	GraphPad	https://www.graphpad.com/scientific-software/prism/ ,RRID:SCR_002798
Sound Recording Software Avisoft-RECORDER	Avisoft	https://www.avisoft.com/recorder.htm , RRID:SCR_014436
MATLAB 2016a	MathWorks	https://www.mathworks.com/products/matlab.html ,RRID:SCR_001622
Other		
Micro-Renathane® Tubing	Braintree Scientific, Inc	MRE-033
Promethion CAB-8 Temperature Control Cabinet	Sables Systems International	N/A
UltraSoundGate 416 USGH	Avisoft Bioacoustics	34163
UltraSoundGate Condenser Microphone CM 16	Avisoft Bioacoustics	40011
2.5 μ L Microliter Syringe Model 62 RN	Hamilton Company	7632-01
32 gauge, Small Hub RN Needle, 15 mm, 15°	Hamilton Company	7803-04
Optic Cannulae	Doric	MFC-400/430-0.48-RM2-FLT
Optic Fibers	Doric	MFP-400/460/1100_FCM-CM2
Attenuator Fiberoptic Patchcode	Doric	MFP-400/430/LWMJ-0.48_FCM-FCM_T0.05
Fluorescence MiniCube	Doric	FMC4_AE(405)_E(460-490)_F(500-550)
LED Driver	Doric	RVP_2CH_1A
405 nm LED	Doric	CLED_405
465 nm LED	Doric	CLED_465
Fiber Photometry Processor	Tucker-Davis Technology	RZ5P
Half & Half cow's milk	Organic Valley	UPC# 0 93966 00033 7

CONTACT FOR REAGENT AND RESOURCE SHARING

Further information and requests for reagents should be direct to and will be fulfilled by the Lead Contact, Marcelo Dietrich (marcelo.dietrich@yale.edu).

EXPERIMENTAL MODELS AND SUBJECT DETAILS

All preweaning mice used in the experiments were 10-21 days old from both genders. Dams used were 2 – 6 months old. In this study, we used the following mouse lines from The Jackson Laboratories: *Agrp^{tm1}(cre)Lowl/J (Agrp^{Cre})* (JAX: 012899); B6;129P2-*Gt(ROSA)26Sortm1(Trpv1,ECFP)Mde/J (R26^{LSL-Trpv1})* (JAX: 008513); B6.129X1-*Trpv1tm1Jul/J (Trpv1^{KO})* (JAX: 003770); B6N.129-*Rpl22tm11Psam/J (Rpl22^{LSL-HA})* (JAX: 011029); 129S-*Npy^{tm1Rpa/J (Npy^{KO})}* (JAX: 004545); and *Slc32a1^{tm1Lowl} (or Vgat^{Flox/Flox})* (JAX: 012897).

Agrp^{TRPV1} mice were: *Agrp^{Cre}tm1/+;Trpv1^{-/-};R26-LSL-Trpv1^{Gt/+}*; control animals were *Trpv1^{-/-};R26-LSL-Trpv1^{Gt/+}* mice injected with capsaicin. *Agrp^{Cre}* and *R26^{LSL-Trpv1}* mice were backcrossed to *Trpv1^{KO}* mice to avoid the peripheral actions of capsaicin when injected systemically to activate *Agrp* neurons (Arenkiel et al., 2008; Dietrich et al., 2015; Güler et al., 2012; Ruan et al., 2014). We have thoroughly characterized *Agrp^{TRPV1}* mice previously (Dietrich et al., 2015). *Agrp^{HA}* mice were generated by crossing *Agrp^{Cre}* to *Rpl22^{LSL-HA}* mice. Analysis of ectopic expression of Cre was performed by using a specific set of primers against the excised conditional allele, as characterized before (Dietrich et al., 2015); mice with ectopic expression of the excised allele were not used in the studies. *Agrp^{Vgat-KO}* mice were generated by crossing *Agrp^{Cre}* to *Vgat^{Flox/Flox}* mice to finally generate *Agrp^{Cre/+};Vgat^{Flox/Flox}*. Controls were Cre negative littermates. All mice were kept in temperature- and humidity-controlled rooms, in a 12/12 hr light/dark cycle, with lights on from 7:00 AM–7:00 PM. Food (Teklad 2018S, Envigo) and water were provided *ad libitum* unless otherwise stated. All procedures were approved by IACUC (Yale University).

METHOD DETAILS

Drugs

capsaicin (10 mg/kg, s.c. or i.p.; 3.33% Tween-80 in PBS; from Sigma) and oxytocin (5mg/kg, 15 IU/mg dissolved in PBS; from Sigma).

Immunohistochemistry

Mice were deeply anesthetized and perfused with freshly prepared fixative (paraformaldehyde 4%, in PBS 1x [pH = 7.4]). Brains were post-fixed overnight in fixative and sectioned on a vibratome. Coronal brain sections (50 μ m) were washed several times in PBS 1x (pH = 7.4) and pre-incubated with Triton X-100 (0.3% in PBS 1x) for 30 min. Sections were then incubated in a blocking solution (Triton 0.3%, Donkey Serum 10%, Glycine 0.3M in PBS 1x) for one hour. Sections were then incubated with rabbit polyclonal anti-Fos (1:200; sc-52, Santa Cruz Biotechnologies) or rabbit monoclonal anti-Fos (1:1000, #2250; Cell Signaling Technology) and mouse polyclonal anti-HA (1:1000; 901503, Biologend) for 16 hr. After, sections were extensively washed in 0.3% Triton in PBS and incubated with secondary fluorescent Alexa antibodies (1:500). Sections were mounted and visualized by a Leica TCS SP5 Spectral Confocal Microscope (Center for Cellular e Molecular Imaging, Yale University). During the entire procedure, investigators were blinded to the experimental groups. The ImageJ analysis program (version 1.51h, NIH, USA) (Girish and Vijayalakshmi, 2004; Schindelin et al., 2012) was utilized to count the number of –HA positive (*Agrp*^{HA} neurons) and Fos-positive neurons manually.

Isolation from the nest (Figures 1A–1D):

At postnatal day 10 (P10), neonates (*Agrp*^{HA}) were divided into three conditions: (1) kept with the biological mother and littermates (nest); (2) isolated for 90 minutes and (3) isolated for 8 hours. Isolated animals were single-housed and placed in a clean chamber with fresh bedding. Pups were sacrificed and expression of Fos was evaluated. Samples were prepared for immunohistochemistry as described above. *Agrp*^{HA} pups were used in these studies to allow identification of *Agrp* neurons. All samples were prepared and counted blinded for the experimental groups.

Milk intake in the nursing nest (Figures 1E and 1F):

when ten days of age (P10), pups were divided into two groups: kept with the biological mother or isolated for 90 minutes. Isolated pups were reintroduced to the biological mother for another 90 minutes after isolation. Body weight was measured prior and after 90 minutes. To ensure that animals within each group had similar milk availability, they were tested using an equal number of animals. Upon reintroduction of the isolated pups to the home cage, pups that stayed with the dam were removed to avoid competition. These experiments were not blinded.

Measurement of corticosterone levels (Figure 1G):

At postnatal day 10, neonates were divided into two groups: kept with the biological mother or isolated for 90 minutes. After testing, neonates were deeply anesthetized, and blood samples were collected through cardiac puncture. A total of 150 μ l of blood was collected. Blood samples were left at room temperature for one hour and centrifuged at 5000 rpm for 20 minutes. Plasma was collected and stored at -80° C. Corticosterone level was measured using an enzyme immunoassay (ELISA) kit (Enzo Life Sciences, Farmingdale, NY, USA) according to the manufacturer's instructions.

Isolation from the nest in the presence of a predator odor (Figures 1H–1J):

At postnatal day 10 (P10), pups (*Agrp*^{HA}) were divided into three conditions: (1) kept with the biological mother and littermates (nest); (2) isolated for 90 minutes and (3) isolated for 90 minutes in the presence of a synthetic predator odor (2,4,5-Trimethylthiazole (mT), Sigma-Aldrich). Isolated animals were single-housed and placed in a clean chamber with fresh bedding. Ten microliters of mT odor were pipetted onto a small square nesting material (2 \times 2 cm). To avoid contact with the odor, the chamber was divided by a wire mesh resulting in two small compartments, allowing the pups to smell the odor.

Isolation from the nest with milk infusion (Figures 1K–1O):

The procedure of milk infusion consisted in the insertion of a polyurethane-based catheter tubing (Micro-Renathane® Tubing, MRE-033, Braintree Scientific, Inc.) attached to a pump. To avoid an invasive procedure, the inserted tube end was heated and bent to create a small U shape at its end tip. After insertion into the mouth, the tube was attached to the fur on the outside of the cheek using a small drop of crazy glue to hold it in place. The whole procedure did not require anesthesia and last less than 30 s. A total of 200 μ l of milk was infused during the 90 minutes (15 μ l ejections, every 5-15 minutes). The following types of milk were used: (1) commercial Half & Half cow's milk (Organic Valley, Ultra Pasteurized Grade A); an (2) mouse milk collected from lactating dams. To confirm that milk was infused, a tasteless blue dye (Erioglaucine disodium salt, Sigma-Aldrich, Cat. 861146) was added (< 1 mg/mL) to the milk prior infusion. The stomach was excised to confirm the blue color indicating milk ingestion.

Mouse milk collection

The milk collection was performed on lactating dams with litters between the ages of P8-P12. Dams were separated from their litter for 6 hours prior collection to ensure adequate milk production. Dams were lightly anesthetized with isoflurane and oxytocin (5 mg/kg, i.p) was administered to promote milk release. Milk was expressed from the nipples using pressure from the thumb and forefinger to gently massage and squeeze the mammary tissue in an upward motion until a visible bead of milk begins to form at the base of the teat. Then, milk was collected using a 20 μ l calibrated pipette, pipetted into a 1.5 mL Eppendorf tube and stored at -20°C until the day of the test. The duration of the milk collection lasts less than 10 minutes.

Artificial feeding protocol (Figures 1P–1R):

when seven days old, neonates were separated from the biological dam and kept with a non-lactating foster dam. Every 3–4 hours, the neonates were separated from the foster dam and milk was provided for \sim 30 minutes by the experimenter using a surrogate nipple attached to a tip in a 100 μ L pipette. The volume of intake in each session varied between 80 μ l to 150 μ l of milk. Because of the limitation in getting mouse milk, we performed the artificial feeding using a more caloric formula of cow milk (Heavy Whipping Cream, Organic Valley) that resembles the nutrition facts of a mouse milk (Görs et al., 2009). At postnatal day 10, milk was provided for 30 minutes and immediately after neonates were separated into two groups: kept with the non-lactating foster dam and littermates (nest) or isolated for 90 minutes. All other procedures for Fos counting were as described above.

Assessment of maternal components with foster dams (Figures 2A–2C):

At postnatal day 10, neonates were separated from the biological dam and placed in the cage of a foster dam. Foster dams in different lactation conditions were used: (1) non-lactating foster dam; (2) non-lactating foster dam with protruded nipples; (3) lactating foster dam. Dam rodents have the nipples still distended without milk release permitting suckling for two weeks after weaning if the female is not pregnant again. Lactating foster dams were chosen in a similar postnatal day of lactation, and their offspring was removed immediately before placing the alien/unfamiliar neonates. Neonates were divided into five groups: (1) kept with the biological dam and littermates (nest); (2) kept with a non-lactating foster dam; (3) kept with a non-lactating foster dam with protruded nipple; (4) kept with lactating foster dam with protruded nipple and (5) isolated for 90 minutes. All other procedures for Fos counting were as described above.

Isolation from the nest with thermal support (Figures 2D–2G):

When ten-day-old, neonates were separated from the biological dam, and thermal support was provided using two different conditions. In the first condition, neonates were placed in a humidity and temperature-controlled climate chamber (70%–80% of humidity, 35°C , Sables Systems). In the second condition, a thermal support device set at 35°C was placed underneath the chamber in which the neonates were separated. We confirmed appropriated thermal conditions by monitoring the temperature throughout testing using calibrated thermometers. Neonates were divided into four groups: (1) kept with the biological dam and littermates (nest); (2) isolated for 90 minutes at thermoneutrality; (3) isolated for 90 minutes in the thermal support device; and (4) isolated for 90 minutes without thermal support (room temperature). All other procedures for Fos counting were as described above.

Isolation from the nest in pups raised at thermoneutrality (Figures 2H–2J):

The lactating dam was placed in a humidity and temperature-controlled climate chamber (70%–80% of humidity, 35°C , Sables Systems) two weeks before delivery to acclimate to the new environment. Temperature and humidity in the climate chamber were monitored twice a day until testing. At postnatal day 10, neonates were divided into three groups: (1) kept with the biological dam and littermates (nest); (2) isolated for 90 minutes at room temperature; and (3) isolated for 90 minutes at thermoneutrality. All other procedures for Fos counting were as described above.

Fiber photometry (Figure 3):

Agrp^{Cre/Cre} mouse neonates (P0–P1) were cryo-anesthetized. Neonates were placed on ice, using aluminum foil as a barrier to prevent direct contact with the ice. After 8 minutes, neonates were removed from the ice and placed onto a chilled rat/mouse neonatal frame (Stoelting Co., Wood Dale, IL). A Cre-dependent adeno-associated virus (AAV) encoding the calcium sensor jRCaMP7s (AAV8-CAG-Flex-jRCaMP7s-SV40, Penn Vector Core) was injected unilaterally at a volume of 300 nL using following coordinates from lambda: AP = +.98 ML, lateral = -0.3mm , DV = -4.1mm . On postnatal day 12, a fiber optic cannula (NA = 0.48, core diameter = 400 μm from Doric Lenses) was placed over the arcuate nucleus using following coordinates from bregma: AP = -1.38 mm , lateral = -0.3mm , DV = -5.8 mm . One to two days after placing the fiber optic cannula, experimental mice were placed in a Plexiglas cage (10 cm x 8 cm x 6 cm) with 4 siblings and bedding from home cage. After 5 minutes of baseline fiber photometry recordings (see below), mice connected to the fiber photometry system were moved to an identical adjacent Plexiglas cage for a period of ten minutes of isolation. Subsequently, experimental mice were return to the cage with the siblings for 5 minutes. The fiber photometry system consisted of two different sets of LEDs: 405 nm LED sinusoidally modulated at 211 Hz and a 460 nm LED sinusoidally modulated at 333 Hz. Both light streams were merged into an optical fiber patch using a minicube (Doric Systems). The fiber optic patch was connected to the cannula on the mouse pup. Fluorescence emitted by jRCaMP7s in response to light excitation was collected with same fiber patch cord and focused into a photodetector (Newport). The signal collected at the photodetector was

collected in a digital fiber photometry processor (RZ5P, Tucker-Davis Technologies). Signal was processed and pre-analyzed using the Synapse Software Suite (Tucker-Davis Technologies). The data were exported to MATLAB for post-processing. First, the isosbestic channel (405 nm excitation) was fitted to the calcium-dependent channel (460 nm excitation, denoted as F) using first order polynomial fitting (F_0 denotes the fitted isosbestic). The calcium fluorescence activity was calculated as: $(F - F_0)/F_0$. The high-frequency components of the fluorescence activity were then filtered out by a low pass filter at 0.5 Hz. We then down sampled the signal by averaging it in non-overlapping windows of 0.1 s. The Z-score was calculated considering the minute before isolation as the baseline.

Recording of ultrasonic vocalizations (Figures 4 and 5):

P10 mice were separated from the dam and placed in a soundproof chamber. In the thermoneutrality experiment, pups were divided into two groups: (1) isolated for 90 minutes at room temperature or (2) isolated for 90 minutes at thermoneutrality (70%–80% of humidity, 35°C, Sables Systems). USVs were recorded for 90 minutes. In experiments with the *Npy*^{KO} and *Agrp*^{Vgat-KO} mice, USVs were recorded for ten minutes immediately following separation from the dam in the soundproof chamber. In the experiment with *Agrp*^{Trpv1} mice, this initial ten minutes was considered as a baseline before activation of *Agrp* neurons. Then, P10 mice were injected with capsaicin (10 mg/kg, s.c) and USVs were recorded for an additional twenty minutes. USVs were recorded using an UltraSoundGate Condenser Microphone CM 16 (Avisoft Bioacoustics, Berlin, Germany) placed 10 cm above the animals. The microphone was connected via an UltraSoundGate 416 USGH audio device and recorded with a sampling rate of 250,000 Hz by the software Avisoft RECORDER (version 4.2.16; Avisoft Bioacoustics).

Maternal preference test (Figures 5N–5P):

The maternal preference test was performed in a three-chamber apparatus (65 × 42 × 23 cm) and comprised of three stages: Stage 1 – acclimation: the dam was allowed to explore the apparatus without the presence of pups for ten minutes. Stage 2 – exploration: two P10 mice (control and *Agrp*^{Trpv1}, $n = 25$ pairs) were placed on each side of the apparatus inside of an inverted metal wire cup and the dam was allowed to explore the pups for ten minutes. Stage 3 – preference: dam was restricted to the center compartment, pups were injected with capsaicin (10 mg/kg, s.c) and placed in the cups and then the dam was allowed to explore all compartments for 20 minutes. Groups were randomly alternated between both sides to avoid preference for one side of the chamber. Time spent interacting with the pups was measured using Any-maze (Stoelting Co., Wood Dale, IL).

Analysis of ultrasonic vocalizations

Ultrasonic vocalizations (USV) were automatically extracted from the audio recordings by using spectral analysis through image processing. Each audio file was analyzed in segments of 1 minute long and then Short Fourier transformed with a Hamming windowing function (window = 256), NFFT = 1024 sampling points and an overlap between successive windows equal to half of the window size. These parameters generate a spectrogram with resolution of 0.5 ms and 244 Hz. The spectrograms were converted to grayscale images and the USVs were segmented on the spectrogram through a sequence of image processing techniques, which included the contrast enhancement of the image ($\gamma = 1$), the application of an adaptive threshold (sensitivity of 20%) followed by a series of morphological operations and identification of connected components. The segmented USV candidates were then analyzed by a local median filtering (LMF) to eliminate segmentation noise based on the contrast between an USV candidate and its background. The minimum contrast acceptable between an USV candidate and its background was automatically estimated based on a differential geometry analysis of the contrast of all the USV candidates detected in an audio recording. USVs less than 10 ms apart were considered as part of the same syllable. Next, all the USVs were classified in 11 distinct call types (Grimsley et al., 2011) by a Convolutional Neural Network, which had the AlexNet architecture as starting point. The network was trained for USV classification with over 14,000 samples of real USVs, which were then augmented in order to increase the variability of the samples, resulting in > 57,000 samples. The output consisted of a table summarizing the main features of the USVs detected. This table contains the start and end time of the USVs, as well as its mean, maximum and minimum frequency, mean intensity and other relevant spectral features such as the existence of harmonic components. Each vocalization received a label based on the most likely call type label attributed by the Convolutional Neural Network. The label of each USV is also available as a probability distribution function over all the call types. The software was custom developed in our laboratory and is available upon request. The details of the software will be published elsewhere.

Mouse pup behavior toward the anesthetized dam (Figures 6A–6G and 7A–7J):

Animals were recorded under infrared illumination and assessed for 20 minutes at postnatal day 10 (P10) and postnatal day 15 (P15). Each animal was tested at one age only. Before the experiment, the dam was anesthetized (100 mg/kg Ketamine + 10 mg/kg Xylazine). The maximum number of pups tested per dam was eight. Animals received an injection of capsaicin (10 mg/kg, s.c.) before the experiment. We used a custom built-chamber (20 × 15 cm built in opaque Plexiglas). The dam was placed at an angle of 45° on her back along the edge. Pups were placed on the other edge of the chamber, ~20 cm away from their dam. Parameters such as latency to attach to the dam's nipple, distance traveled, and the number of nipple attachments were assessed using Any-Maze (Stoelting Co., Wood Dale, IL). Experiments were performed blinded for the genotype.

Mouse pup behavior toward the anesthetized dams injected with oxytocin (Figures 6P–6V and 7K–7P):

In anesthetized dams, milk ejection is largely decreased, and dams are considered non-lactating (Lincoln et al., 1973). To circumvent this issue, we performed a similar experiment as described above but injected the anesthetized dams with oxytocin (5 mg/kg, i.p) immediately before each test. Nipples were manually expressed to confirm that there was milk ejection before the experiment. P10 mice received an injection of capsaicin (10 mg/kg, s.c) and were subsequently assessed for 20 minutes. In this assay, a second injection of oxytocin (5 mg/kg, i.p) was given at 10 minutes of test. P15 mice received an injection of capsaicin (10 mg/kg, s.c) and were subsequently assessed for 10 minutes. The duration of the testing period was shorter because P15 mice quickly attached to the dam's nipple in preliminary experiments. Parameters such as latency to attach to the dam's nipple, distance traveled, and the number of nipple attachments were analyzed using Any-Maze (Stoelting Co., Wood Dale, IL). Body weight was measured prior and after testing. Experiments were performed blinded for the genotype.

Independent feeding (Figures 7Q and 7R):

Mice were tested at postnatal days P15, P18, and P21. Naive animals were used for each postnatal age and mice were acclimated to the behavior room for one-hour before the experiment. Food was left inside the cage to prevent a state of deprivation. Animals were tested in a mouse cage filled with home bedding and two Petri dishes placed in opposite corners. After the acclimation period (1 hour), the experiment was performed. Animals were removed from the cage, received an injection of capsaicin (10 mg/kg, i.p.) and were returned to the cage. One Petri dish was empty; the other had a pellet of chow diet. Body weight and food intake were evaluated after 30 minutes. Experiments were performed blinded for the genotype.

QUANTIFICATION AND STATISTICAL ANALYSIS

MATLAB (2016a or above) and Prism 8.0 were used to analyze data and plot figures. All figures were edited in Adobe Illustrator CS6/CC. Illustrations were designed by Mind the Graph (MindtheGraph.com). Data were first subjected to a normality test using the D'Agostino & Pearson normality test or the Shapiro-Wilk normality test. When homogeneity was assumed, a parametric analysis of variance test was used. The Student's t test was used to compare two groups. Welch's correction was used when standard deviations were unequal between groups. ANOVA was used to compare multiple groups. Tukey-Kramer's multiple comparisons test was used to find post hoc differences among groups and calculate 95% confidence intervals to report effect size. When 95% confidence intervals were not calculated, then the Holm-Sidak's multiple comparisons test was used. When homogeneity was not assumed, the Kruskal-Wallis nonparametric ANOVA was selected for multiple statistical comparisons. The Mann-Whitney U test was used to determine significance between groups. Two sample Kolmogorov–Smirnov test was used to calculate the statistical differences between features of ultrasonic vocalizations. Chi-square test was used to find differences in the number of pups that attached to nipples in the behavior tests performed in neonates. One- or two-tail tests were used based on prior experimental hypothesis. Statistical data are provided in text and in the figures. In the text, values are provided as mean \pm SEM $p < 0.05$ was considered statistically significant.

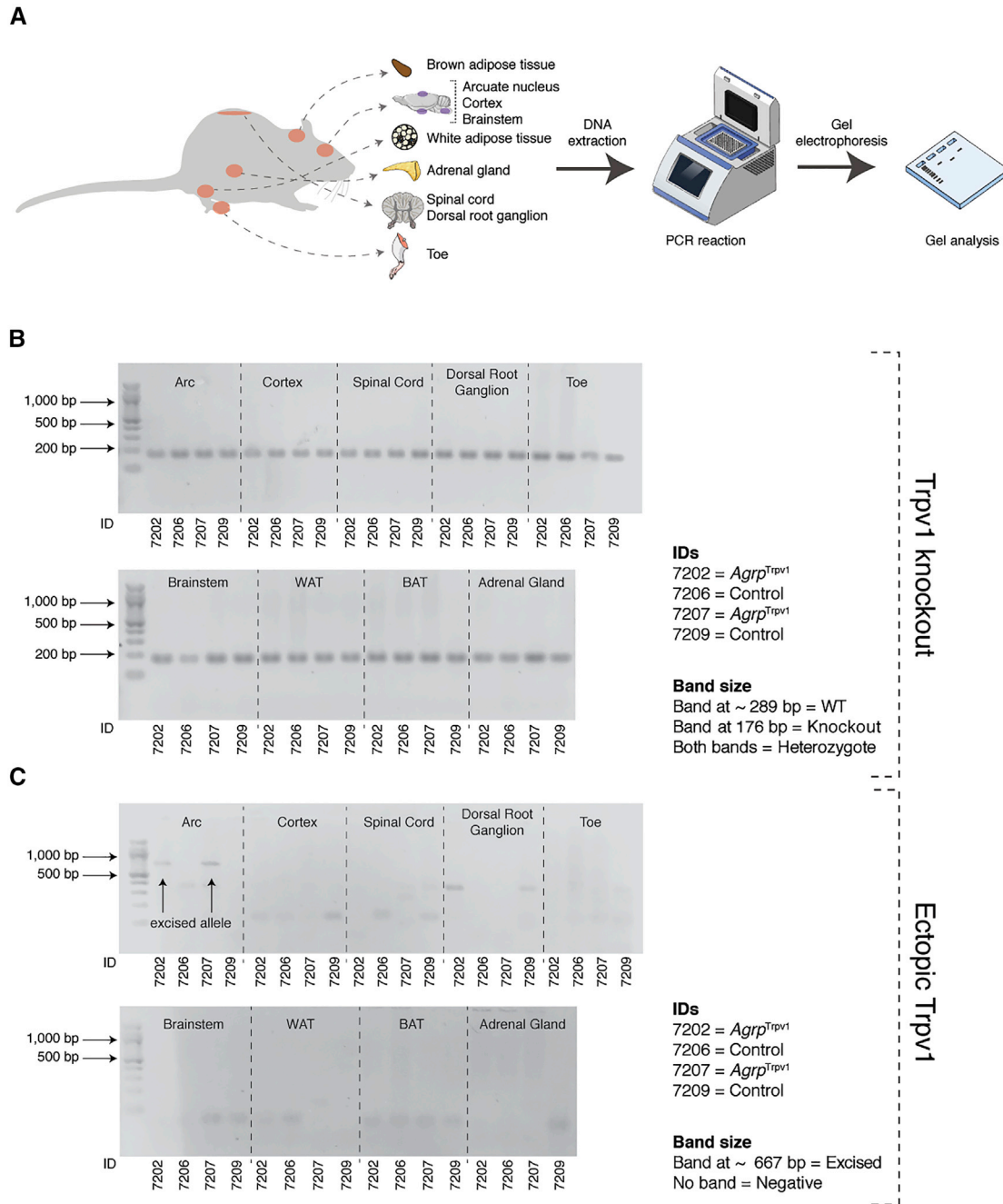


Figure S1. PCR-Based Analysis for Genotyping *Agrp^{trpv1}* and Control Mice, Related to Figure 5

(A) Illustrative diagram of the tissue collection and PCR-based analysis genotyping.

(B) Genomic DNA samples from P15 mice were extracted and amplified using primers for *Trpv1* knockout allele. The lower band is the knockout allele for the *Trpv1* gene.

(C) Genomic DNA samples from P15 mice were extracted and amplified using primers for ectopic *Trpv1* allele. The upper band (667 bp) shows that the excised allele for *Trpv1* is specifically expressed in the arcuate nucleus of the hypothalamus.